Evidence of haze-driven secondary production of supermicrometer aerosol nitrate and sulfate in size distribution data in South Korea

Joseph S. Schlosser[1], Connor Stahl[1], Armin Sorooshian[1,2], Yen Thi-Hoang Le[3], Ki-Joon Jeon[3,4,5], Peng Xian[6], Carolyn E. Jordan[7,8], Katherine R. Travis[7], James H. Crawford[7], Sung Yong Gong[9], Hye-Jung Shin[10], In-Ho Song[10], Jong-sang Youn[5,11]

[1]Department of Chemical and Environmental Engineering, University of Arizona, Tucson, Arizona, USA
[2]Department of Hydrology and Atmospheric Sciences, University of Arizona, Tucson, Arizona, USA
[3]Program in Environmental and Polymer Engineering, Inha University, 100 Inha-ro, Incheon 22212, Republic of Korea.
[4]Department of Environmental Engineering, Inha University, 100 Inha-ro, Incheon 22212, Republic of Korea.
[5]Particle Pollution Research and Management Center, Incheon 21999, Republic of Korea
[6]Marine Meteorology Division, Naval Research Laboratory, Monterey, CA, USA
[7]NASA Langley Research Center, Hampton, VA, USA
[8]National Institute of Aerospace, Hampton, VA, USA
[9]Climate, Air Quality and Safety Research Group/Division for Atmospheric Environment, Korea Environment Institute, 370 Sicheong-daero, Sejong 30147, Republic of Korea
[10]Air Quality Research Division, Climate and Air Quality Research Department, National Institute of Environmental Research, 42 Hwangyoun-ro, Incheon 22689, Republic of Korea
[11]Department of Energy and Environmental Engineering, the Catholic University of Korea, 43 Jibong-ro, Bucheon 14662, Republic of Korea

Correspondence to: Jong-sang Youn (jsyoun@catholic.ac.kr) and Armin Sorooshian (armin@arizona.edu)

Abstract. This study reports measurements of size-resolved aerosol composition at a site in Incheon along with other aerosol characteristics for contrast between Incheon (coastal) and Seoul (inland), South Korea, during a transboundary pollution event during the early part of an intensive sampling period between 4 and 11 March 2019. Anthropogenic emissions were dominant in the boundary layer over the study region between 4 and 6 March, with much smaller contributions from dust, smoke, and sea salt. The meteorology of this period (shallow boundary layer, enhanced humidity, and low temperature) promoted local heterogeneous formation of secondary inorganic and organic species, including atypically high nitrate (NO_3^-) relative to sulfate (SO_4^{2-}). Seoul exhibited higher $PM_{2.5}$ levels than Incheon likely due to local emissions. The following findings point to secondary aerosol formation and growth sensitivity to water vapor during this pollution event: (i) significant concentrations of individual inorganic and organic acids in the supermicrometer range relative to their full size range (~40%) at higher humidity; (ii) high correlation (r = 0.95) between oxalate and SO_4^{2-}, a marker of secondary aqueous production of oxalate; (iii) increased sulfur and nitrogen oxidation ratios as a function of humidity; and (iv) matching composition apportionment (for soluble ions) between the PM_1 and $PM_{2.5-1}$ size fractions. The last finding confirms that PM_1 aerosol composition measurements fully capture $PM_{2.5}$ composition apportionment (for soluble ions) during haze events and, therefore, may be reliably applied in modeling studies of such events over the full $PM_{2.5}$ size range. The study period was marked by relatively low temperatures that made NO_3^- the most abundant species detected, pointing to the sensitivity of $PM_{2.5}$ levels and composition as a function of season during such transboundary events. For instance, other such events in previous studies exhibited more comparable levels between SO_4^{2-} and NO_3^- coincident with higher temperatures than the current study. This dataset can contribute to future evaluation of model $PM_{2.5}$ composition to better support regulatory efforts to control $PM_{2.5}$ precursors.

1 Introduction

South Korea has been the focus of extensive air quality research in recent years owing to continuing challenges as it is a growing metropolitan center with extensive sources of pollution both locally and regionally (Lee and Kim, 2007;Guttikunda et al., 2003). Although direct emission control policies have reduced primary pollutant concentrations over time (e.g., lead, carbon monoxide, sulfur dioxide), there has been less success to reduce levels of secondarily formed pollutants associated with particulate matter with diameters (D) less than or equal to 2.5 μm ($PM_{2.5}$) (Kim and Lee, 2018). A common phenomenon leading to significant aerosol concentrations over large parts of South Korea is transboundary pollution events stemming from areas such as China (Choi et al., 2019b;Choi et al., 2019a;Peterson et al., 2019;Lee et al., 2019b;Eck et al., 2020;Cha et al., 2019) that impact both coastal and inland parts of the peninsula. These events include dust (Heim et al., 2020;Kim et al., 2012), industrial and agricultural burning emissions (Lamb et al., 2018), sea salt (Lee et al., 2018), and wildfire plumes from Siberia (Lamb et al., 2018) that are superimposed on the local pollution sources that include biogenic emissions, urban and vehicular emissions, shipping emissions, industrial activities, and biomass burning (Park et al., 2021;Lamb et al., 2018).

While the influence of long-range transport on the Korean peninsula's air quality has been demonstrated (Lee et al., 2021;Koo et al., 2018), a question remains about the relative contributions of transboundary versus local emissions. Results from the Megacity Air Pollution Studies-Seoul (MAP-Seoul) study (May – June 2015) indicated that advected pollution from China mostly affects western coastal sites and that local emissions are significant in accounting for Seoul's radiation-absorbing aerosol particles (Lee et al., 2018). Others have pointed to the importance of domestic emissions during transboundary pollution events, especially when transport rates are below ~250 km day^{-1} (Lee et al., 2019b). Studies from the Korea-United States Air Quality (KORUS-AQ) campaign (1 May – 10 June 2016) showed that during transboundary pollution episodes, Seoul (inland) exhibited significantly higher levels of $PM_{2.5}$ than coastal areas (Eck et al., 2020). Nault et al. (2018) showed with in-situ measurements that local emissions are the primary contributor to secondary organic aerosol (SOA) over Seoul. Furthermore, diurnal variations in aerosol optical depth (AOD) are also more significant at inland sites versus coastal sites (Lennartson et al., 2018). In their analysis of the same pollution episode as our study in early March 2019, Lee et al. (2019a) showed that the foreign contribution to $PM_{2.5}$ in Seoul was 78.8% as compared to 21.2% from domestic sources based on the Community Multiscale Air Quality (CMAQ) model. It is important to note that such apportionments are sensitive to the modeled composition of $PM_{2.5}$ as discussed in Choi et al. (2019a) and Jordan et al. (2020). Hence, comparisons of measured and modeled $PM_{2.5}$ composition are needed to validate apportionment between domestic and transported pollutants.

Local and upwind meteorology have been shown to play a major role in modulating temporal trends in PM and gas pollutant levels over South Korea (Seo et al., 2018;Cho et al., 2021;Jordan et al., 2020;Koo et al., 2020;Peterson et al., 2019;Ryu et al., 2021). Models have yet to adequately capture sulfate (SO_4^{2-}) formation in East Asian haze events (Shao et al., 2019) as they generally underestimate SO_4^{2-} in haze, while the KORUS-AQ study also revealed that nitrate (NO_3^-) formation in haze may be simultaneously overestimated resulting in errors in aerosol liquid water content and other modeled properties (Jordan et al., 2020). Other recent studies of East Asian haze have pointed to the importance of secondary aerosol formation, primarily ammonium sulfate and nitrate salts, with additional SOA (Hu et al., 2014;Huang et al., 2014;Cheng et al., 2016;Li et al., 2018;Zhang et al., 2017). Moisture and thus aerosol-laden water have been shown to be especially important to promote the formation of these secondary species (Wu et al., 2018;Zhang et al., 2018;Wang et al., 2016;Zhang et al., 2017). The May-June 2016 period of KORUS-AQ offered a detailed view of frontal passages transporting pollution from China to the Korean peninsula under cloudy and humid conditions that promoted haze and fog formation within a shallow stable boundary layer (Jordan et al., 2020;Peterson et al., 2019). Sulfate and NO_3^- formation was observed to be efficient owing to heterogeneous processing with the former fueled by local and transported sulfur dioxide (SO_2) and the latter from local nitrogen oxides (NO_x) and enhanced nocturnal NO_3 radical reactions. A positive feedback was suggested whereby increased water uptake by particles increased gas-to-particle partitioning, which in turn further increased water uptake. Furthermore, clouds reduced transmission of solar radiation to the surface, thereby reducing mixing and leading to more PM accumulation in a shallow boundary layer. Jordan et al. (2020) called for more detailed aerosol and meteorological measurements co-located with AirKorea sites (https://www.airkorea.or.kr/eng) that routinely monitor $PM_{2.5}$ and other basic pollutants (PM_{10}, O_3, SO_2, NO_2, CO) in order to advance knowledge of aerosol lifecycle behavior over the Korean peninsula.

Aerosol composition provides important evidence for impacts of meteorology and atmospheric circulation on PM, which are sometimes challenging to reproduce in models. The current study exploits an Incheon dataset of size-resolved composition during a major pollution episode in March 2019 to expand on the evidence for these impacts and to help interpret observations from the larger network of ongoing Korean observations. Data were collected at both Incheon near the western coast of South Korea and at the inland city of

106 Seoul (Fig. S1), which allows for a critical look at how $PM_{2.5}$ levels compare between the sites and if Seoul has
107 higher levels (suggesting local $PM_{2.5}$ production) as described by Eck et al. (2020) and Jordan et al. (2020). This
108 study examines the role for meteorological parameters like humidity in impacting size-resolved aerosol
109 composition. This is especially important since past studies have mainly focused on bulk PM_1, $PM_{2.5}$ or PM_{10}
110 (Park et al., 2018;Ryu and Min, 2021;Seo et al., 2018;Won et al., 2020). Size-resolved composition data are
111 pertinent to improve understanding of how particles in the region impact cloud formation, visibility, and public
112 health, all of which are sensitive to size-specific aerosol properties.

113
114 **2 Datasets and Methods**
115   During the period between 4 and 11 March 2019, there was a major regional haze pollution event that
116 impacted Incheon and Seoul monitoring sites. The haze event lasted for approximately the first three days and
117 then the air quality improved between 7 and 11 March (Fig. 1). We consider the period from 4 March 10:00 – 6
118 March 19:00 as "polluted", from 6 March 19:00 – 7 March 09:15 as "transition", and 7 March 09:15 – 11 March
119 10:00 as "clean"; these time definitions are chosen based on start/stop times of size-resolved impactor
120 measurements conducted in Incheon (Sect. 2.1.1) during periods with higher, intermediate, and lower PM
121 concentrations (e.g., Fig. 1). Times in this study are in Korea standard time (KST), where KST = UTC + 9 hours.
122 This study relies on a variety of datasets summarized below.
123
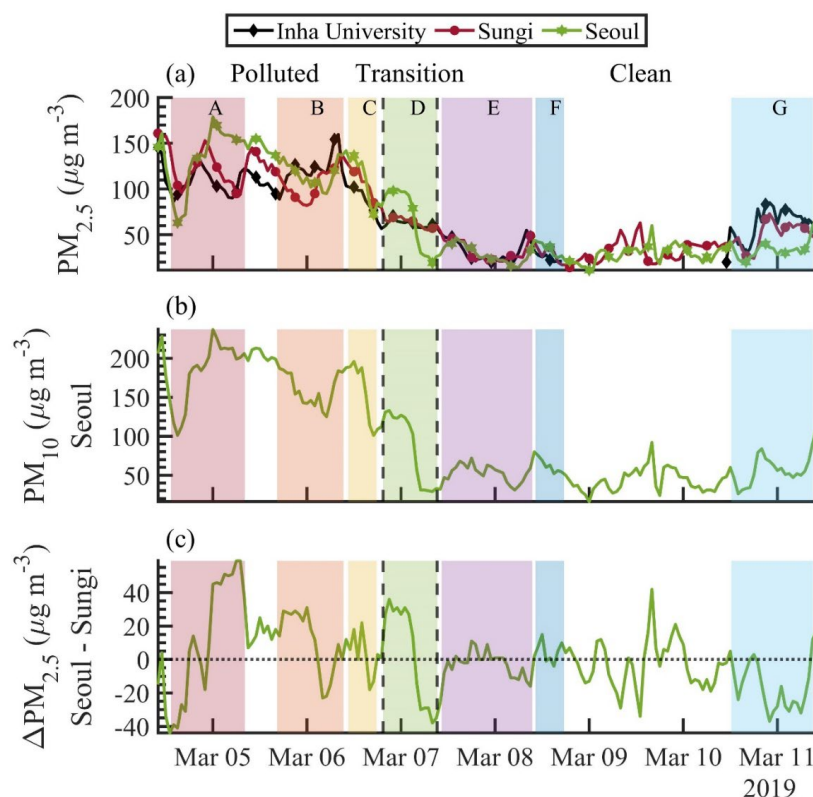
125 **Figure 1. Time series of the following parameters: (a) $PM_{2.5}$ measured at Inha University, Sungi, and Seoul;**
126 **(b) PM_{10} measured at Seoul; and (c) $PM_{2.5}$ difference between Seoul and Sungi. The dashed black vertical**
127 **lines separate the (left) polluted, (middle) transition, and (right) clean periods. The horizontal line in (c)**
128 **denotes a $PM_{2.5}$ difference of zero to clearly show positive and negative deviations from that value. Shaded**
129 **regions are labeled with individual DLPI+ sets (see Table 2) overlapping in time.**
130

2.1 Aerosol and Gas Monitoring

The focus of this study is on three specific monitoring sites in Incheon and Seoul, which were compared to a wide network of other stations in those cities to confirm agreement in temporal variability and concentrations. Incheon has a population of 2,936,367 in contrast to Seoul having 9,565,990 (Korea, 2021). The three primary sites include Inha University and Sungi in Incheon, and the Seoul Intensive Monitoring Station (hereafter referred to as Seoul site) in Seoul (locations in Fig. S1). Measurements at these sites are described below and summarized in Table 1. Figure S1 shows the location of the other 17 and 40 National Ambient air quality Monitoring Information System (NAMIS) stations in Incheon and Seoul, respectively, which were operational during the study period with data provided online by AirKorea; Sungi is one of those sites in Incheon but the Inha and Seoul sites are not part of that network. The rationale for including two primary sites in Incheon is because Inha provided unique data not typically measured by NAMIS, and Sungi was closest to Inha among the NAMIS options. Furthermore, the Seoul site had very comprehensive measurements itself and thus it was sufficient for this study.

Table 1. Sample site name, latitude and longitude coordinates of each site, and the parameters measured at each site.

Site	Latitude	Longitude	Measurements
Incheon: Inha University	37°27'2.08"N	126°39'20.87"E	Aerosol: $PM_{2.5}$, 467/528/652 nm wavelength absorption coefficient (α), size-resolved particulate mass samples
Incheon: Sungi	37°27'34.74"N	126°39'27.31"E	Aerosol: $PM_{2.5}$ Gas: Ozone (O_3), nitrogen dioxide (NO_2), carbon monoxide (CO), sulfur dioxide (SO_2)
Incheon Meteorological Site	37°28'39.85"N	126°37'28.40"E	Meteorological: Ambient temperature (T), wind speed and direction, ambient relative humidity (RH), ambient pressure (P), rain
Seoul Intensive Monitoring Station	37°36'38.40"N	126°56'1.36"E	Aerosol: PM_{10}, $PM_{2.5}$; speciated $PM_{2.5}$ concentrations of sulfate (SO_4^{-2}), nitrate (NO_3^-), chloride (Cl^-), sodium (Na^+), ammonium (NH_4^+), potassium (K^+), magnesium (Mg^{2+}), calcium (Ca^{2+}), organic carbon (OC), elemental carbon (EC), silicon (Si), titanium (Ti), vanadium (V), manganese (Mn), iron (Fe), nickel (Ni), copper (Cu), zinc (Zn), Arsenic (As), selenium (Se), lead (Pb) Gas: SO_2, NO_2, O_3, CO Meteorological: T, wind speed and direction, RH, P, rain

2.1.1 Inha University (Incheon)

Aerosol composition measurements were conducted on a building rooftop (300 m ASL; 37° 27' 2.08"N, 126° 39' 20.87"E) on the Inha University campus, which is a residential area ~3 km away from Incheon harbor. Three instruments were operated simultaneously during the study period from 4 March 2019 to 11 March 2019. Real-time $PM_{2.5}$ measurements were conducted using an optical particle counter (OPC-Grimm model 1.109, Grimm Aerosol Technik, Germany) with 1 min time resolution. Real-time monitoring of light absorbing aerosol particles was conducted with a tricolor absorption photometer (TAP model 2901, Brechtel Mfg. Inc., USA), which monitors light absorption by particles on a filter at three wavelengths (467, 528, 652 nm). In this study we focus on 652 nm data for simplicity. Lastly, size-resolved particulate matter samples were collected on Teflon filters (PTFE support, 0.1 μm pore, 25 mm, Zefon International) using a low pressure impactor (DLPI$^+$, Dekati, Finland) with aerodynamic lower cutpoint diameters of 0.016, 0.030, 0.054, 0.094, 0.15, 0.25, 0.38, 0.60, 0.94, 1.6, 2.5, 3.6, 5.3, and 10 μm. Daily filter sets were collected on the seven days of the sampling period with details shown in Table 2. Temperature and relative humidity varied slightly between sets (Table 2) with potential impacts on size of particles owing to hygroscopic growth and evaporation/condensation (e.g., Chen et al., 2018). As temperatures were low (4.5-9.1°C on average), evaporation is likely negligible. There was more potential for hygroscopic growth during the polluted and transition periods (66-79% RH) as compared to the clean period (47-52% RH), and this does not alter conclusions of this work as size shifts owing to water uptake are an important aspect of understanding regional haze events in the study region. Note as well that hygroscopic influences on size cut-off shifts in cascade impactors are most important for RHs above 80% and when sea salt is dominant (Chen et al., 2018), which do not apply to this study. Particles were extracted from the filters in 10 mL of deionized

167 water and placed in ultrasonic bath at 30°C for 60 min for subsequent analysis with ion chromatography (IC,
168 Thermal Scientific Dionex ICS-2100 system) to speciate anions and cations.
169
170 **Table 2. Summary of the DLPI$^+$ sample sets including sample set name, pollution category, the start and**
171 **end date in Korea standard time (KST = UTC + 9 hr), as well as the sample averages of T, wind speed and**
172 **direction, RH, and P. Sample flow rate was 9.71 L min^{-1} for all sample sets.**

Set	Pollution Category	Start Time (KST)	End Time (KST)	T (°C)	Wind Speed (m s^{-1})	Wind Direction (°)	RH (%)	P (hPa)
A	Polluted	3/4/2019 13:21	3/5/2019 08:10	7.2	3.0	236	79	1009
B	Polluted	3/5/2019 16:24	3/6/2019 09:19	6.4	1.7	224	74	1010
C	Polluted	3/6/2019 10:32	3/6/2019 17:48	9.1	2.7	307	66	1007
D	Transition	3/6/2019 19:26	3/7/2019 09:15	4.5	3.9	221	75	1008
E	Clean	3/7/2019 10:21	3/8/2019 09:28	5.7	2.9	295	52	1014
F	Clean	3/8/2019 10:19	3/8/2019 17:34	8.9	3.2	244	47	1017
G	Clean	3/10/2019 12:14	3/11/2019 09:08	8.3	2.8	220	51	1002

173
174 The IC analysis has been described in other works (Stahl et al., 2020;MacDonald et al., 2018;Cruz et
175 al., 2019), with limits of detection (LOD) for each species examined shown in Table S1. Values measured below
176 the LOD are replaced with LOD/2, with the percent of such samples per species provided in Table S1. For anion
177 analysis, an AS11-HC 250 mm column and potassium hydroxide eluent were used with the following gradient
178 program with a suppressor (AERS 500e) current of 28 mA: begin at 2 mM, increase to 8 mM from 0 to 20 minutes,
179 and then increase from 8 to 28 mM from 20 to 30 minutes. Cation analysis involved a CS12A 250 mm column
180 and methanesulfonic acid eluent with the following program with a suppressor (CERS 500e) current of 22 mA:
181 start at 5 mM, isocratic from 0 to 13 minutes, increase from 5 to 18 mM from 13 to 16 minutes, and then isocratic
182 at 18 mM from 16 to 30 minutes. Sample concentrations were corrected using background sample concentrations
183 for individual species, which included sodium (Na$^+$), ammonium (NH$_4^+$), potassium (K$^+$), magnesium (Mg^{2+}),
184 calcium (Ca^{2+}), chloride (Cl$^-$), NO$_3^-$, SO$_4^{2-}$, methanesulfonate (MSA), adipate, maleate, oxalate, and phthalate.
185 The latter five species were summed in parts of the analysis and referred to as "organic acids" with the caveat that
186 they represent the dissociation anion of either sulfonic or organic acids.
187 Concentrations for SO$_4^{2-}$, Mg^{2+}, K$^+$, and Ca^{2+} refer to their non-sea salt (NSS) values based on
188 calculations relying on the measured concentrations of Na$^+$ and its ratio with these species in pure sea salt (Seinfeld
189 and Pandis, 2016). The mean percentage of sea salt mass removed for those four species relative to total speciated
190 mass of each filter set (excluding the sea salt portion of those four species) was 2%. Those species for which more
191 than 15% of samples were below the LOD (i.e., Mg^{2+}, maleate, phthalate, adipate, MSA) are not discussed on an
192 individual basis in this study but are used in calculations dependent on the cumulative dataset such as the overall
193 charge balance; the exception is bromide (Br$^-$), which is fully removed from calculations as it was always below
194 the LOD.
195
196 **2.1.2 Sungi Site (Incheon)**
197 We use PM$_{2.5}$, O$_3$, CO, NO$_2$, and SO$_2$ data at one hour time intervals collected at Sungi (41 m ASL; 37°
198 27' 34.74"N, 126° 39' 27.31"E) by NAMIS. These parameters are measured based on the following methods:
199 PM$_{2.5}$ = Beta-ray absorption method (BAM; MetOne Ins.), SO$_2$ = pulsed ultraviolet fluorescence method, CO =
200 non-dispersive infrared method, NO$_2$ = chemiluminescent method, O$_3$ = ultraviolet photometric method. The gases
201 were monitored by Teledyne API products (SO$_2$ = 100E, NO$_2$ = 200E, O$_3$ = 300E, CO = 400E). Of note is that the
202 PM$_{2.5}$ measured at Sungi and Inha University with independent techniques generally agreed well during the study
203 period (Fig. 1) with a coefficient of determination (R^2) of 0.82.
204

2.1.3 Seoul Intensive Monitoring Station

Gas and aerosol (PM_{10} and $PM_{2.5}$) data are used from the Seoul site (67 m ASL; 37° 36' 38.40"N, 126° 56' 1.36"E), which is independent from the NAMIS network. The following parameters were measured: $PM_{2.5}$ and PM_{10} = Beta-ray absorption method (BAM), ionic species concentrations (SO_4^{2-}, NO_3^-, Cl^-, Na^+, NH_4^+, K^+, Mg^{2+}, Ca^{2+}) = Ambient Ion Monitor (URG 9000D, URG Co.) and ion chromatography (Dionex, DX-1 000; IonPac AS14A and the CS12A columns), organic carbon (OC) and elemental carbon (EC) = semi-continuous OC/EC analyzer (Sunset Laboratory) based on the thermal/optical reflectance (TOR) method, elemental concentrations (Si, Ti, V, Mn, Fe, Ni, Cu, Zn, As, Se, Pb) = online X-ray fluorescence (XRF) analyzer (Xact-420, Cooper Environmental Co.), SO_2 = pulsed ultraviolet fluorescence method, CO = non-dispersive infrared method, NO_2 = chemiluminescent method, O_3 = ultraviolet photometric method. Gases were monitored with the same techniques as at the Sungi site. All speciated aerosol information at Seoul are for $PM_{2.5}$.

2.2 Meteorological data

Meteorological data for winds, temperature (T), pressure (P), relative humidity (RH), and rain were used from monitoring stations in Incheon and Seoul. The Korea Meteorology Administration provided data from an Automated Synoptic Observing System (ASOS) for the Incheon station (37° 28' 39.85"N, 126° 37' 28.40"E) (kma.go.kr), which is located ~5 km northwest of the Inha University sampling site. Meteorological data were collected at the same site described for Seoul in Sect. 2.1.3. Specific humidity (q) was calculated using measured values of T, P, and RH (Bolton, 1980).

Planetary boundary layer height (PBLH) data are used from Modern Era Retrospective-analysis for Research and Application version 2 (MERRA-2) (Gelaro et al., 2017). MERRA-2 uses the Goddard Earth Observing System Data Assimilation System Version 5 (GEOS-5) and is hosted and maintained by the National Aeronautics and Space Administration (NASA) Global Modeling and Assimilation Office (GMAO). The MERRA-2 PBLH product is provided as part of the surface flux diagnostics dataset (GMAO, 2015). The resolution of the PBLH product is 0.5° x 0.625° and is assimilated on an hourly timescale. All four sample sites described above are within the same grid point (37.500°N, 126.875°E) in the MERRA-2 PBLH product.

2.3 Trajectory and Chemical Transport Modeling

We use the NOAA HYSPLIT model (Rolph et al., 2017; Stein et al., 2015) for air mass back-trajectory information. We rely on the Global Data Assimilation System (GDAS) at 0.5° × 0.5° resolution and the model vertical velocity method for treating vertical motion. Four day back-trajectories were calculated for each hour between 4 – 11 March 2019. We use an ending altitude of 500 m AGL at the Inha University sampling site, which was sufficient to represent the predominant sources impacting the various sample sites during the week of focus owing to their close proximity. This ending altitude has proved to be successful for other surface air quality studies in other regions (e.g., Aldhaif et al., 2021; Crosbie et al., 2014; Mora et al., 2017; Hersey et al., 2015) and nearby in southeast Asia (e.g., AzadiAghdam et al., 2019). We obtained data for the following parameters along trajectories: ambient temperature (°C), rainfall (mm hr^{-1}), mixed layer depth (m), RH (%), and downward solar radiation flux (W m^{-2}).

For large-scale background aerosol information we rely on the Navy Aerosol Analysis and Prediction System (NAAPS) (Lynch et al., 2016) accessible at https://www.nrlmry.navy.mil/aerosol/. We specifically use the reanalysis version of NAAPS, called NAAPS-RA. This is a chemical transport model with 25 vertical levels using a terrain-following sigma-pressure coordinate system that provides data in 1° × 1° grids every 6 hours. The model is driven by the Navy Global Environmental Model (NAVGEM) for meteorological information (Hogan et al., 2014). The final reanalysis results are created after assimilating Moderate Resolution Imaging Spectroradiometer (MODIS) and Multi-angle Imaging Spectro Radiometer (MISR) data into the model (Zhang and Reid, 2006; Hyer et al., 2011). Reanalysis output is provided for dust, sea salt, open biomass burning smoke, and "anthropogenic and biogenic fine (ABF)" that includes secondarily produced species (i.e., SO_4^{2-}, primary organic aerosols, and SOA) mainly confined to the fine mode (< 1 μm).

3 Time Series of PM Concentrations

March 2019 was characterized by a major transboundary pollution event impacting the Korean peninsula with visual satellite imagery (Fig. S2) clearly showing the presence and then absence of significant haze. Owing to their proximity to one another, the Inha and Sungi stations in Incheon revealed similar values and changes in $PM_{2.5}$ ($R^2 = 0.82$ for the full study period) with a significant reduction from polluted (~115 μg m^{-3}) to transition (~63 μg m^{-3}) and clean (~40 μg m^{-3}) periods (Table 3 and Fig. 1). Both Inha and Sungi $PM_{2.5}$ levels were strongly correlated with the mean of data from 17 NAMIS stations across Incheon (Fig. S1: R^2 of 0.82 and 0.98, respectively).

262
263 **Table 3. Average Incheon meteorological, aerosol, and gas parameters for the polluted, transition, and clean**
264 **time periods, with standard deviations shown in parentheses. Times in KST: Polluted = 4 March 10:00 – 6**
265 **March 19:00; Transition = 6 March 19:00 – 7 March 09:15; Clean = 7 March 09:15 – 11 March 10:00.**
266 **Speciated concentrations from Inha represent mass for particles with diameters above 0.016 μm (i.e., full**
267 **size range of DLPI+ sampler) and are weighted by sample duration when calculating the time period**
268 **average; species with concentrations below their respective LOD in more than 50% of samples (see Table**
269 **S1) are not shown. Standard deviations are not shown for the transition period speciated data owing to**
270 **there only being one sample set.**

Site	Parameter	Polluted	Transition	Clean
Incheon Meteorological Site	T (°C)	7.5 (2.1)	4.7 (1.0)	6.7 (3.2)
	Wind Speed (m s^{-1})	2.5 (0.9)	3.7 (1.3)	2.6 (1.2)
	Wind Direction (°)	247 (45)	236 (150)	219 (126)
	RH (%)	73 (15)	77 (8)	51 (20)
	q (g kg^{-1})	4.63 (0.61)	4.07 (0.64)	2.95 (0.81)
	P (hPa)	1009 (2)	1008 (1)	1011 (5)
	PBLH (km)	0.45 (0.56)	1.87 (1.28)	0.53 (0.63)
	Rain (mm)	0 (0)	0 (0)	0 (0)
Inha University	PM$_{2.5}$ (μg m^{-3})	110 (17.9)	61.8 (3.9)	43.6 (20.7)
	α (Mm^{-1})	18.9 (5.1)	11 (1.9)	8.6 (3.1)
	NO$_3^-$ (μg m^{-3})	32.2 (12.1)	10.3 (-)	3.2 (1.1)
	NH$_4^+$ (μg m^{-3})	19.2 (7.7)	8.2 (-)	5.6 (3.8)
	SO$_4^{2-}$ (μg m^{-3})	15.4 (5.2)	7.0 (-)	1.8 (0.6)
	K$^+$ (μg m^{-3})	0.7 (0.3)	0.7 (-)	0.2 (0.05)
	Ca^{2+} (μg m^{-3})	2.0 (0.4)	1.9 (-)	1.7 (0.6)
	Cl$^-$ (μg m^{-3})	2.0 (1.1)	1.6 (-)	0.8 (0.1)
	Na$^+$ (μg m^{-3})	1.1 (0.2)	1.5 (-)	0.8 (0.1)
	Oxalate (μg m^{-3})	0.7 (0.4)	0.3 (-)	0.2 (0.01)
Sungi	PM$_{2.5}$ (μg m^{-3})	117.3 (20.5)	64.6 (6.6)	36.2 (14.1)
	CO (ppm)	0.927 (0.197)	0.800 (0.068)	0.578 (0.154)
	NO$_2$ (ppm)	0.045 (0.019)	0.032 (0.014)	0.037 (0.016)
	O$_3$ (ppm)	0.037 (0.016)	0.031 (0.011)	0.027 (0.016)
	SO$_2$ (ppm)	0.007 (0.002)	0.006 (0.001)	0.008 (0.004)

271
272   Meanwhile, ~30 km farther inland at Seoul, both PM$_{10}$ and PM$_{2.5}$ dropped at a similar rate as Incheon
273 between the three periods (Table 4 and Fig. 1): PM$_{10}$ = ~176 μg m^{-3}, ~91 μg m^{-3}, ~50 μg m^{-3}; PM$_{2.5}$ = ~127 μg
274 m^{-3}, ~71 μg m^{-3}, ~31 μg m^{-3}. The Seoul site PM$_{2.5}$ data were strongly correlated with the 40 NAMIS stations
275 across Seoul (Fig. S1: R^2 = 0.96). Based on the three period averages, Seoul exhibited slightly higher PM$_{2.5}$
276 levels in the polluted and transition periods whereas Incheon was higher during the clean period. The time series
277 of hourly PM data in Fig. 1 shows that near the end of the clean period there was an increase in pollution levels,
278 which is consistent with HYSPLIT data showing back-trajectories shifting from northerly for most of the clean
279 period to northwesterly (i.e., from the Beijing area) (Fig. 2). The R^2 value between PM$_{2.5}$ hourly data was 0.75
280 and 0.82 for Seoul-Inha and Seoul-Sungi, respectively. Although there was decent agreement, differences are

281   apparent in the $PM_{2.5}$ hourly time series (Fig. 1c) with Seoul's levels being significantly enhanced during parts
282   of the polluted and transition periods. The difference in $PM_{2.5}$ between Seoul and Incheon suggests enhanced
283   local production promoting large differences between hourly $PM_{2.5}$ over Seoul versus Incheon, with the
284   maximum difference observed being nearly 50 µg m^{-3} on 5 March, with an average difference that day of 37 ±
285   24 µg m^{-3}.

286
287   **Table 4. Average meteorological, aerosol, and gas parameters for the polluted, transition, and clean time**
288   **periods measured at the Seoul sampling site, with standard deviations shown in parentheses. Note that**
289   **organic aerosol (OA) concentration was calculated by multiplying the OC concentration by a factor of 1.8**
290   **(i.e., OA = OC × 1.8).**

Parameter	Polluted	Transition	Clean
T (°C)	9.3 (3.0)	5.7 (2.0)	7.6 (4.2)
Wind speed (m s^{-1})	1.9 (0.8)	1.8 (1.0)	1.6 (1.0)
Wind direction (°)	240 (59)	261 (104)	178 (128)
RH (%)	55 (17)	69 (5)	36 (14)
q (g kg^{-1})	3.80 (0.66)	3.87 (0.31)	2.17 (0.64)
P (hPa)	1018 (3)	1016 (1)	1019 (5)
PBLH (km)	0.45 (0.56)	1.87 (1.28)	0.53 (0.63)
Rain (mm)	0 (0)	0 (0)	0 (0)
PM_{10} (µg m^{-3})	176.0 (35.0)	90.8 (43.8)	50.3 (16.6)
$PM_{2.5}$ (µg m^{-3})	127.2 (27.5)	70.6 (32.5)	30.5 (9.9)
$PM_{10}/PM_{2.5}$	1.39 (0.09)	1.27 (0.12)	1.69 (0.38)
NO_3^- (µg m^{-3})	43.3 (12.0)	17.3 (9.1)	7.1 (3.4)
NH_4^+ (µg m^{-3})	21.7 (5.0)	11.1 (5.2)	3.2 (1.3)
SO_4^{2-} (µg m^{-3})	19.8 (4.2)	12.3 (5.7)	2.5 (1.3)
OA (µg m-3)	17.0 (3.9)	15.3 (5.6)	10.0 (3.4)
OC (µg m^{-3})	9.4 (2.1)	8.5 (3.1)	5.6 (1.9)
EC (µg m^{-3})	2.9 (0.7)	2.2 (0.8)	1.2 (0.5)
Cl^- (µg m^{-3})	1.4 (0.6)	0.7 (0.3)	0.5 (0.2)
K^+ (µg m^{-3})	0.3 (0.1)	0.2 (0.1)	0.12 (0.05)
Ca^{2+} (µg m^{-3})	0.2 (0.1)	0.08 (0.04)	0.07 (0.03)
Na^+ (µg m^{-3})	0.12 (0.04)	0.04 (0.02)	0.05 (0.03)
Mg^{2+} (µg m^{-3})	0.08 (0.01)	0.03 (0.02)	0.02 (0.02)
Fe (ng m^{-3})	447 (94)	243 (125)	185 (70)
Si (ng m^{-3})	422 (201)	222 (131)	84 (72)
Zn (ng m^{-3})	113 (40)	47 (22)	47 (33)
Pb (ng m^{-3})	42 (10)	34 (17)	15 (7)
Mn (ng m^{-3})	28 (7)	14 (8)	10 (5)
Ti (ng m^{-3})	23 (6)	13 (6)	10 (3)
Cu (ng m^{-3})	14 (7)	6 (3)	8 (6)
V (ng m^{-3})	8 (5)	3 (2)	1 (1)
As (ng m^{-3})	7 (2)	8 (6)	3 (2)
Se (ng m^{-3})	4 (1)	2 (1)	1 (1)
Ni (ng m^{-3})	3 (2)	1 (1)	0.5 (0.5)
CO (ppm)	1.104 (0.175)	1.036 (0.145)	0.655 (0.139)
O_3 (ppm)	0.038 (0.018)	0.029 (0.012)	0.023 (0.016)

NO$_2$ (ppm)	0.037 (0.014)	0.030 (0.013)	0.038 (0.016)
SO$_2$ (ppm)	0.007 (0.001)	0.005 (0.000)	0.006 (0.002)

291
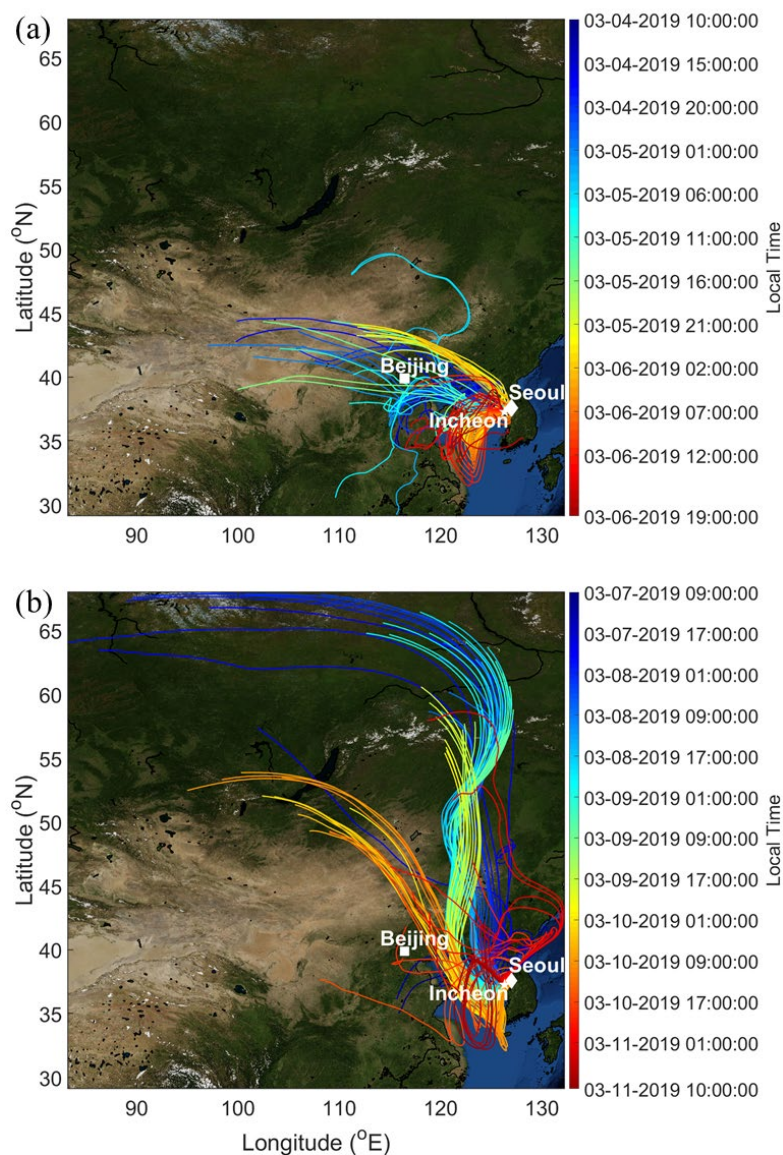
293 **Figure 2. Four-day back-trajectories based on hourly data during the (a) polluted and (b) the clean portion**
294 **of the study period. The ending point of trajectories is at 500 m AGL at Incheon, with environmental**
295 **parameters along the trajectories summarized in Fig. S5. Images retrieved from**
296 **https://worldview.earthdata.nasa.gov/.**
297

298   The $PM_{10}:PM_{2.5}$ ratio is helpful to examine whether a divergence in values occurs that would suggest a
299 strong source of dust as compared to typical background conditions. More specifically, higher values of this ratio
300 could potentially suggest enhanced dust influence owing to mass concentrations of dust being abundant above 2.5
301 μm. As PM_{10} was only measured at Seoul, Table 4 compares the mean (± standard deviation) value of this ratio
302 for the three time periods: polluted = 1.39 ± 0.09, transition = 1.27 ± 0.12, clean = 1.69 ± 0.38. As will be discussed
303 more subsequently, dust did not drive the high PM concentrations during the polluted period, but rather it was
304 driven in large part by secondarily produced species (i.e., SO_4^{2-}, NO_3^-, NH_4^+) that grew into the 1 – 2.5 μm range.
305

4 PM Composition

4.1 PM$_{2.5}$ Composition

308   Speciated $PM_{2.5}$ data from Seoul (Table 4) reveal that the largest contributor was NO_3^- during the
309 polluted and transition periods, with an average during the polluted period of 43.3 μg m^{-3}. Estimating OA mass
310 from the measured mass concentration of OC (OA [μg m^{-3}] = 1.8 × OC [μg m^{-3}] (Zhang et al., 2005)) indicates
311 that OA dominated the $PM_{2.5}$ mass during the clean period followed by NO_3^-. Of all species measured in Table 4,
312 SO_4^{2-} exhibited the highest relative enhancement during the polluted period versus the clean period (factor of
313 7.9), whereas NH_4^+ and NO_3^- were enhanced by factors of 6.8 and 6.1, respectively. OA was only enhanced by a
314 factor of 1.7. In terms of mass concentrations, the difference between the polluted and clean periods for the sum
315 of nitrate, sulfate, and ammonium was 72 μg m^{-3} versus the difference in OA of 7 μg m^{-3} (Table 4). The change
316 in OA is < 10% of the change in the three major inorganic ions.
317   The strong enhancement of the inorganic constituents owes most likely to rapid production (both
318 locally and in transport) in contrast to transported PM that was already produced upwind; the latter would tend
319 to increase OA along with inorganic constituents more comparably than what was observed. In lesser abundance
320 were Cl^-, Na^+, K^+, Mg^{2+}, and Ca^{2+}, which are linked to sea salt and dust (Seinfeld and Pandis, 2016) and thus
321 expected to have appreciable concentrations above 2.5 μm. In terms of the elemental species, the most prevalent
322 species in all three periods were the crustal tracer species Si and Fe, which were 5.0 and 2.4 times higher in
323 concentration, respectively, during the polluted period versus the clean period (Table 4). Most of the crustal
324 tracer species showed enhancements ranging from 1.8 – 2.8. Only Si, Se, and V showed greater enhancement
325 ratios with the latter two enhanced by factors of 4 and 8, respectively.
326   The sum of the $PM_{2.5}$ components using OC in Table 4 accounted for 79% (polluted), 75%
327 (transition), and 68% (clean) of the total $PM_{2.5}$, which is partly due to unmeasured species and that OC includes
328 only the carbon mass and not other elements associated with organic compounds. Using OA instead of OC
329 yields improved $PM_{2.5}$ closure: 85% (polluted), 85% (transition), 83% (clean). This decent level of closure may
330 be largely attributed to the high relative abundance of more easily measured inorganic species, predominantly
331 NO_3^-, SO_4^{2-}, and NH_4^+.
332

4.2 Mass Size Distributions

334   The mass size distribution measurements in Incheon provide a unique look into a typical transboundary
335 pollution event, with the ability to contrast it to the subsequent transition and clean periods. Insights gathered from
336 this analysis have direct relevance to Seoul owing to close proximity to Incheon with the exception of any
337 additional aerosol processing and formation that took place between Incheon and Seoul, including especially
338 Seoul itself. Charge balance details can be found in Sect. S1 and Fig. S3, with a general anion deficit during the
339 study period, including anions not speciated with the IC technique such as various types of organics.
340   Figure 3 summarizes size-resolved composition for the polluted, transition, and clean periods of this
341 study. Ions typically associated with primary natural aerosol sources such as sea salt and dust (Arimoto et al.,
342 1992;Seinfeld and Pandis, 2016), including Ca^{2+}, Na^+, and Cl^-, did not exhibit any significant enhancement during
343 the polluted period (cumulative mass concentrations in Table 3), with varying size distribution peaks based on the
344 species and period during the study. In contrast, the ions linked to secondary formation via gas-to-particle
345 conversion processes (i.e., SO_4^{2-}, NO_3^-, NH_4^+, and organic acids) were dramatically enhanced during the polluted
346 period compared to the clean period (Fig. 3) with the transition in between. These species exhibited their highest
347 concentrations during the polluted period between 0.38 and 3.60 μm, a range which includes larger sizes for these
348 secondarily produced species (especially SO_4^{2-} and NH_4^+) as compared to other regions where their peaks are
349 reported to be between 0.3 and 0.6 μm (Maudlin et al., 2015;Cruz et al., 2019). During the transition period, the
350 inorganic species exhibited maximum concentrations for particles with diameters between 0.38 and 1.60 μm. The
351 clean period was generally marked by these species exhibiting peak concentrations for particles between 0.25 and
352 0.38 μm with a secondary peak from 0.6 and 0.94 μm, albeit neither is pronounced.
353   The likely formation pathway for SO_4^{2-}, NO_3^-, NH_4^+, and organic acids in the polluted period was
354 secondary production, which was assisted in part by high humidity as discussed in more detail in Sect. 6.2. Their

355   common formation mechanism is supported by significant correlations (r ≥ 0.94) during the polluted period
356   between SO_4^{2-}, NO_3^-, NH_4^+, and oxalate, with the latter being the most abundant organic acid during the entire
357   study period but especially in the polluted period (~70% of organic acid mass). The strong correlation between
358   oxalate and SO_4^{2-} during the polluted period is important as a strong correlation between these species (in the
359   absence of biomass burning) is considered a marker for secondary aqueous aerosol formation (Ervens et al.,
360   2004;Yu et al., 2005;Zhou et al., 2015;Hilario et al., 2021a). Oxalate is produced efficiently via aqueous-phase
361   chemistry (Sorooshian et al., 2007;Sorooshian et al., 2006;Wonaschuetz et al., 2012).
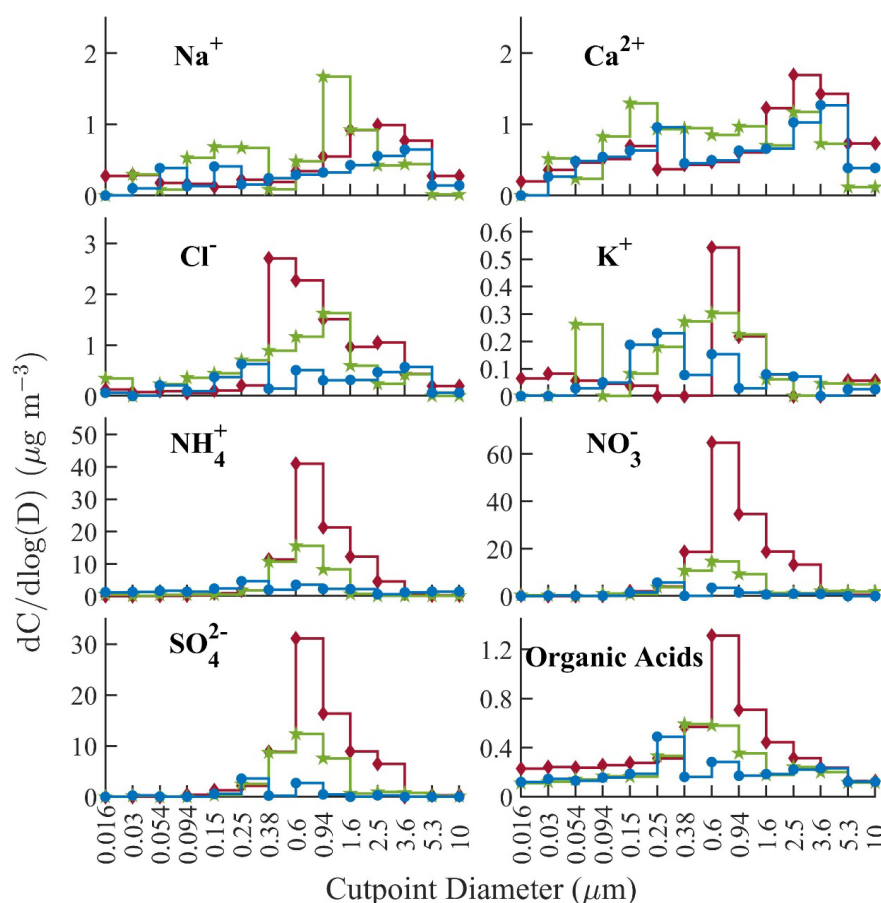
364   Figure 3. Size-resolved composition dC/dlog(D) for (red) polluted, (green) transition, and (blue) clear
365   sample periods. Organic acids = sum of MSA, adipate, maleate, oxalate, phthalate. Sample set data were
366   weighted by sample duration for the polluted and clean periods (note: transition period had just one set).
367   Species that were below LOD in more than 50% of samples (see Table S1) are not shown.

368
369   We next examine if NH_3 was completely neutralized by HNO_3 and H_2SO_4. A charge balance between
370   SO_4^{2-}, NO_3^-, and NH_4^+ can indicate complete neutralization with a slope of unity, as has been tested by other
371   studies (e.g., Lee et al., 2003). A charge balance using individual stages of the three polluted sets collected at Inha
372   University (NH_4^+ on y-axis) between these three species (Fig. S4) yielded a best-fit line slope and y-intercept of
373   1.34 and −0.02, respectively (R^2 = 0.99, n = 20). Our data reveal an anion deficit and that there was sufficient

374 NH_3 to fully neutralize HNO_3 and H_2SO_4. Furthermore, there likely was limited interaction of these acidic gases
375 with coarse particles (e.g., dust and sea salt) that were relatively low in abundance.
376
377 **5 Regional Conditions Influencing PM**
378 **5.1 Atmospheric Circulation and Meteorology**
379   According to previous meteorological analysis (Park et al., 2020a), the airmass history for the polluted
380 period was influenced by the interaction between a Siberian high-pressure system and a migratory anticyclone
381 system, which were located over the Korean peninsula. From 28 February to 1 March 2019, a high-pressure system
382 was located to the west and low-pressure systems were located to the east, all conspiring to yield westerly and
383 northwesterly winds. Lee et al. (2019a) examined a similar time period (27 February – 7 March 2019) and
384 suggested that pollution between 3 – 5 March was transported to the Seoul area at low and high altitudes from the
385 Shandong Peninsula and Beijing, respectively. Pollution levels were exacerbated over South Korea due to a weak
386 high pressure system lingering over the Korean peninsula between 2 and 5 March (Park et al., 2020a). This is
387 evident from the HYSPLIT back-trajectories (Fig. 2a) showing airmasses moving slower in the polluted period
388 versus the subsequent clean period (Fig. 2b). Following the lingering period, a low-pressure system moved in over
389 Russia associated with more clouds and rain upwind of the sampling sites (Fig. S5). There were stronger winds
390 that were northerly between 7 and 11 March. In both the polluted and clean periods, air masses descended from
391 ~2.5 – 4 km four days earlier to within the mixing layer (Fig. S5). The NAAPS spatial maps of speciated optical
392 depths (Fig. S6) and surface mass concentrations (Fig. S7) confirm the spatial extent of the regional haze event
393 extending from the Korean peninsula to areas like Beijing with the ABF (Anthropogenic and Biogenic Fine =
394 SO_4^{2-}, primary organic aerosols, and SOA) component being most prominent during the study period and the
395 driver of the polluted period enhancements in PM, consistent with the dominance of SO_4^{2-}, NO_3^-, and NH_4^+ from
396 the in-situ measurements.
397   The local weather conditions at both Incheon (Table 3) and Seoul (Table 4) exhibited the following
398 common characteristics: (i) generally low average temperatures (< 10°C) that decreased after the polluted period;
399 (ii) low average wind speeds (2.5 – 3.7 m s^{-1} in Incheon, < 2 m s^{-1} in Seoul); iii) highest mean PBLH during the
400 transition period (1.87 m compared to ≤ 0.53 m for the other periods); (iii) lowest average humidity in the clean
401 period (RH ≤ 51% and q ≤ 2.95 g kg^{-1}); and (iv) negligible rain. Although locally there was negligible rain, there
402 was some precipitation along the trajectories arriving at these sites in the polluted and clean periods (Fig. S5),
403 with some potential to reduced aerosol concentrations via wet removal. The time series of these various
404 environmental conditions at Incheon and Seoul are shown in Fig. S8 and demonstrate high temporal similarity
405 and the similar characteristics noted above. The relatively low regional wind speeds during the polluted period
406 (Figs. 2 and S8) indicate that transport was slow allowing for the accumulation and persistence of the haze over
407 this whole domain.
408
409 **5.2 Gas Concentrations**
410   Gases (CO, O_3, NO_2, SO_2) exhibited fairly similar values (Tables 3-4) and temporal patterns (Fig. S9)
411 between Sungi and Seoul, with CO exhibiting the largest relative reduction between successive periods, followed
412 by O_3. $PM_{2.5}$ only exhibited a strong relationship with CO at Sungi and Seoul based on correlation coefficients
413 during the full study period (r = 0.84 and 0.87, respectively). As CO is tracer for anthropogenic emissions
414 (Fishman and Seiler, 1983), its high correlation with $PM_{2.5}$ at both sites supports the strong influence of
415 anthropogenic aerosol at both sites. The reduction of CO from the polluted to the clean period is possibly due to
416 Chinese influence; in contrast to South Korea, combustion efficiency has been shown to be worse in China
417 (Halliday et al., 2019), which supports the high CO levels during the polluted period with air masses coming from
418 China. CO is commonly used in calculations related to aerosol transport studies (e.g., Dadashazar et al.,
419 2021;Hilario et al., 2021b) as it is relatively insensitive to wet scavenging processes with a long lifetime in the
420 atmosphere (~1 month) compared to aerosol particles (Weinstock, 1969).
421
422 **6 Evidence for Enhanced Local Secondary Aerosol Production**
423 **6.1 Differences Between Seoul and Incheon**
424   We now consider $PM_{2.5}$ differences between Incheon and Seoul, where the latter exhibits elevated levels
425 during most of the polluted period (Fig. 1). KORUS-AQ research highlighted that while transport brings aerosol
426 particles from upwind sources, high humidity and cloudiness concentrates local pollution in a shallow stable
427 boundary layer, which promotes secondary aerosol production (Jordan et al., 2020). Jordan et al. (2020) showed
428 that Seoul exhibited $PM_{2.5}$ levels that were on average ~10 μg m^{-3} higher than those at Incheon during the
429 transport/haze period of KORUS-AQ that persisted for 7 days. The maximum daily mean enhancement of $PM_{2.5}$
430 in Seoul from Incheon over that period was 24 μg m^{-3}, while the peak hourly mean enhancement reached 32 μg

431   m^{-3}. These observations were attributed plausibly to more local emissions in Seoul. The same explanation arguably
432   applies to a large extent in our study period too, where the mean difference during the polluted period between
433   Seoul and Incheon $PM_{2.5}$ was 10 µg m^{-3} for Sungi and 17 µg m^{-3} for Inha (Tables 3 and 4) with the peak hourly
434   enhancement between Seoul and Sungi nearly 60 µg m^{-3} (Fig. 1). Here again, humidity (both q and RH) is elevated
435   and PBLH is low compared to the subsequent clean period when PM levels were drastically lower. As the two
436   sites are quite close to one another (~ 30 km), the most likely explanation for higher PM levels at Seoul is more
437   local emissions rather than additional aging to produce secondary aerosol species via transport.
438
439   **6.2 Role of Humidity**
440   The relative fraction of SO_4^{2-}, NO_3^-, NH_4^+, and organic acids in the supermicrometer range (i.e.,
441   technically $D \geq 0.94$ µm) as compared to all sizes sampled at Inha ($D \geq 0.016$ µm) during the polluted period was
442   43%, 44%, 42%, and 36%, respectively, which is appreciable and potentially influenced by the humid conditions.
443   More specifically, it is hypothesized that in the polluted period there was both hygroscopic growth of particles
444   and additional chemical uptake in those swollen particles with enhanced aerosol-laden water to promote higher
445   concentrations of these secondary species.
446   Of the meteorological parameters shown in Tables 3-4, $PM_{2.5}$ levels at Inha University, Sungi, and Seoul
447   were best correlated with q (r = 0.66, 0.64, and 0.78, respectively) across the entire study period. The second-best
448   relationship was with RH (r = 0.53, 0.47, and 0.53, respectively) with minimal relationships with either
449   temperature (r: 0.02 – 0.17) or wind speed (-0.29 ≤ r ≤ 0.13). This motivates an examination of the relationships
450   between PM and humidity to assess the plausibility of a role for heterogeneous secondary aerosol production from
451   local and transported gas-phase precursors.
452   One metric used to quantify such enhanced aerosol production is the oxidation ratio, specifically the
453   sulfur and nitrogen oxidation ratios (SOR and NOR, respectively) where SOR = $SO_4^{2-}/(SO_4^{2-} + SO_2)$ and NOR =
454    $NO_3^-/(NO_3^- + NO_2)$ (Colbeck and Harrison, 1984). Higher values of SOR and NOR indicate that the gaseous
455   precursors form higher relative amounts of SO_4^{2-} and NO_3^-, respectively (Kaneyasu et al., 1995). Previous studies
456   have reported increased SOR and NOR as a function of RH in several locations throughout China that includes
457   Nanjing, Beijing, Hangzhou, and Xi'an (Zhang et al., 2021;Quan et al., 2015;Wu et al., 2018;Huang et al., 2020;Ji
458   et al., 2018). In particular, Huang et al. (2020) showed that SOR increased exponentially with aerosol water
459   content when RH > 50% in Beijing during polluted periods in the wintertime. Given our finding that q is better
460   correlated with $PM_{2.5}$ than RH, we compare SOR and NOR to q (Fig. 4). We evaluate these ratios for our Seoul
461   data only as all the requisite data were measured at the same site. The mean (± standard deviation) of NOR and
462   SOR during the three time periods of the study were as follows (NOR/SOR): polluted = 0.39 ± 0.1/0.51 ± 0.06;
463   transition = 0.22 ± 0.10/0.44 ± 0.14; clean = 0.09 ± 0.04/0.14 ± 0.07. We find a positive relationship between
464   NOR and SOR with q(RH), with R^2 values being 0.58(0.24) and 0.82(0.43), respectively. For context, during a
465   polluted period in Xi'an, China, NOR and SOR values were 0.32 and 0.33, respectively, with high R^2 values with
466   aerosol water content (NOR = 0.55; SOR = 0.81) (Zhang et al., 2021). While the average q and RH were slightly
467   higher for the transition period in Seoul relative to the polluted period (Table 4), the peak values of q, RH, SOR,
468   and NOR all occurred during the beginning of the polluted period (Fig. S10).
469   This study's results suggest there was significant heterogeneous processing to produce species like SO_4^{2-},
470   NO_3^-, NH_4^+, and organic acids above ~1 µm. These species accounted for ~93% of the total speciated ion mass at
471   Inha during the polluted period (Table 3) and are strongly correlated with one another (0.93 ≤ r ≤ 1.00).
472   Heterogeneous production of inorganic species such as SO_4^{2-} in cloudy and humid conditions is common for the
473   study region (Jeon et al., 2021;Jordan et al., 2020;Park et al., 2020b). Furthermore, significant secondary
474   production of SO_4^{2-} above 1 um at high RH has been noted in Beijing (Wang et al., 2020). Mechanisms potentially
475   responsible include aqueous oxidation by O_3, H_2O_2, and transition-metal ion-catalyzed O_2, and also heterogeneous
476   oxidation on surfaces of aerosol particles and droplets via the same oxidants (Li et al., 2020). Table 4 shows that
477   at Seoul the concentrations of elements such as Fe, Cu, Zn, and Pb were higher during the polluted period, which
478   is assumed to be similar at Incheon, supporting the possibility of transition metal-catalyzed secondary production
479   of secondary SO_4^{2-}. Enhanced aerosol liquid water in more humid conditions also promotes partitioning of species
480   to the aerosol-phase as has been documented for NO_3^- in the study region (Seo et al., 2020) and is common for
481   organic acid precursors (Hennigan et al., 2008;Hennigan et al., 2009;Sorooshian et al., 2010). The increased total
482   concentration of NH_4^+ in the polluted period relative to the clean period and strong correlation with SO_4^{2-}, NO_3^-,
483   and oxalate is related to its key role in salt formation (Paciga et al., 2014;Seinfeld and Pandis, 2016;Zhang et al.,
484   2015).
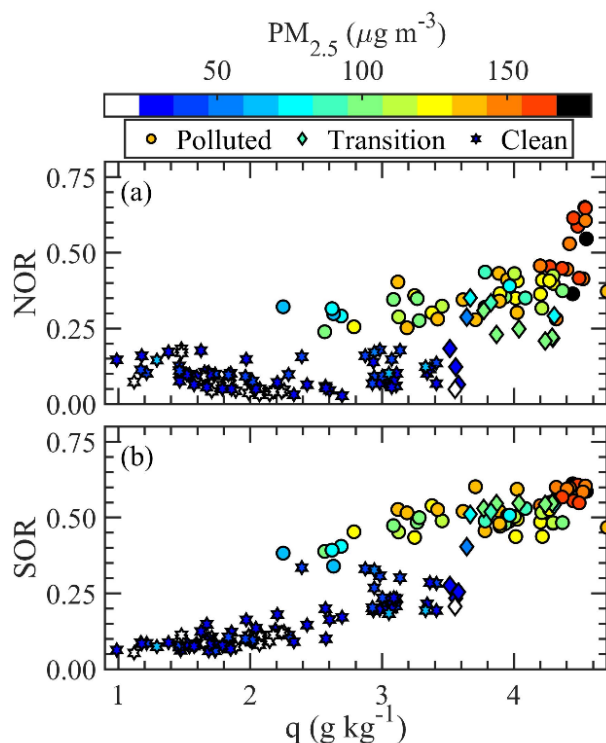
486
487 **Figure 4. (a) Nitrogen oxidation ratio (NOR) and (b) sulfur oxidation ratio (SOR) as a function of q based**
488 **on hourly Seoul data. Points are colored by PM₂.₅ with shapes assigned to the three time periods in the study.**
489

490 **6.3 Does PM₁ Composition Represent PM₂.₅ Composition?**
491   The size-resolved composition data in Incheon allows for a comparison of how the composition of
492 $PM_{0.94}$ differs from the fraction of remaining material contributing to $PM_{2.5}$ (denoted $PM_{2.5-0.94}$). Figure 5 shows
493 that while the transition and clean periods exhibit differences between the apportionment of the mass between
494 $PM_{0.94}$ and $PM_{2.5-0.94}$, during the polluted period the composition is essentially the same. This supports the
495 argument that the presence of supermicrometer secondary inorganic species derives from the same processes the
496 give rise to those compounds in $PM_{0.94}$. Hence, composition measurements using instruments that exclude
497 supermicrometer particles can be used to investigate the composition and evolution of East Asian haze events.
498 Further, models can reliably apply PM_1 composition apportionment to the full $PM_{2.5}$ size range in their assessments
499 of sources and mitigation strategies for these events. A cautionary note is that these implications apply when PM
500 is dominated by inorganics, as with our case, with a limitation of our analysis being the lack of comprehensive
501 size-resolved OC measurements. However, the differences evident in the transition and clean periods imply that
502 under other atmospheric conditions PM_1 composition measurements will not fully reflect the apportionment of
503 $PM_{2.5}$ aerosols. Another important conclusion from Fig. 5 is that the relative amount of $PM_{2.5-0.94}$ versus $PM_{0.94}$
504 was highest in the polluted period (39% of speciated $PM_{2.5}$ vs. 28% for transition and 21% for clean), further
505 reinforcing that there was increased production of secondarily formed inorganic species in the coarse mode.
506
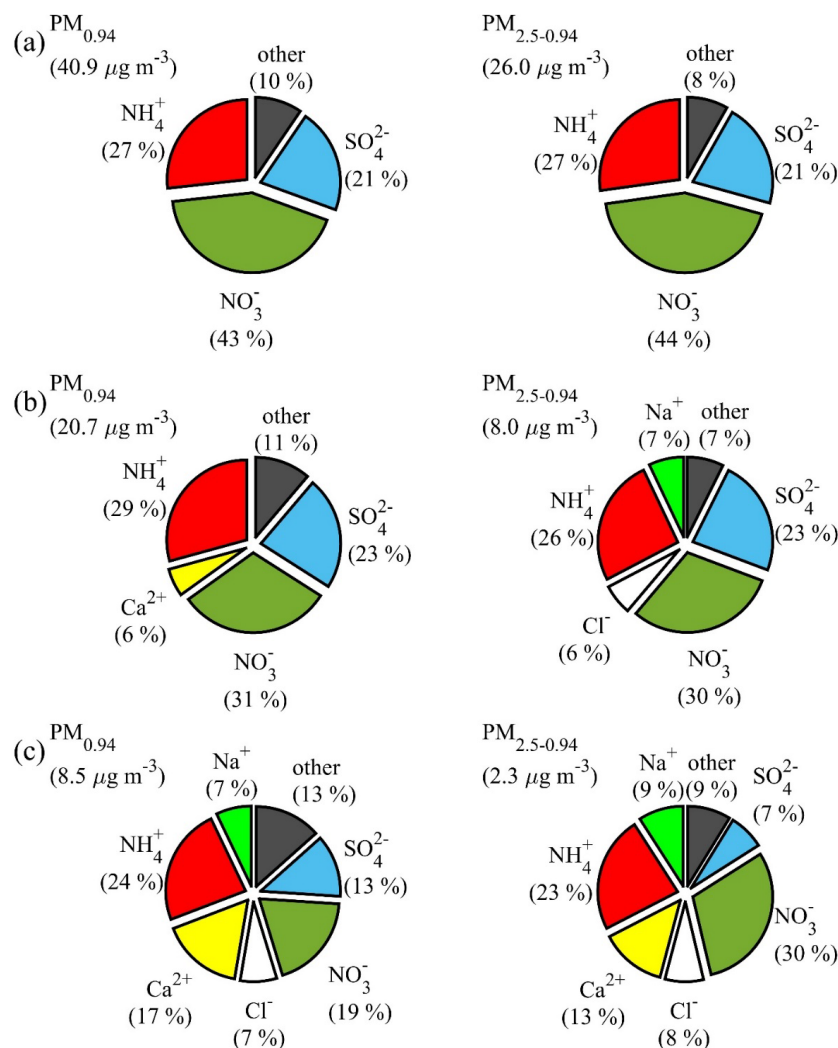
Figure 5. Percent composition of (left panels) PM$_{0.94}$ and (right panels) particulate mass between 0.94 and 2.50 μm (PM$_{2.5-0.94}$) for the (a) polluted, (b) transition, and (c) clean periods. Any parameter with percent mass composition ≤ 5% is grouped into the 'other' category of each diagram. Mean mass concentrations associated with PM$_{0.94}$ and PM$_{2.5-0.94}$ for the three time periods (weighted by sample duration for each period) are provided next to each pie.

6.4 Atypically High Nitrate

Contrasting this pollution event with another one investigated during KORUS-AQ (May – June 2016) points to a surprising difference in the relative amount of NO_3^- versus SO_4^{2-} (Jordan et al., 2020). The KORUS-AQ event exhibited comparable amounts between the two species. Compared to that event's concentrations, NO_3^- is about an order of magnitude larger in this study, while SO_4^{2-} is only about a factor of two greater. Gas-phase SO_2 is comparable between the two events. The difference is most likely explained by the much lower temperatures in the March 2019 event relative to the other study, which is thermodynamically more favorable for

521 HNO$_3$ partitioning to the particle phase to increase NO$_3^-$ levels (Seinfeld and Pandis, 2016). The ratio NO$_3^-$:SO$_4^{2-}$
522 based on the full size distribution of the Inha filter sets was ~2.1 during the polluted period, where for the Seoul
523 PM$_{2.5}$ data the ratio was ~2.2. The relative production of NO$_3^-$ relative to SO$_4^{2-}$ likely varies seasonally with colder
524 temperatures and higher humidity more conducive to higher NO$_3^-$ and thus PM$_{2.5}$ levels. High NO$_3^-$ events are not
525 particularly common, as shown especially for Beijing (Yang et al., 2017), requiring favorable conditions such as
526 cold temperatures, high humidity, a shallow boundary layer, and high precursor levels. These factors all conspired
527 together in the March 2019 transboundary pollution event to yield such high NO$_3^-$ levels.
528
529 **7 Conclusions**
530   This work relies on a unique set of data collected during a major transboundary pollution event that
531 impacted the Korean peninsula in March 2019. In-situ gas, aerosol, and meteorological data are compared between
532 Incheon (coastal) and Seoul (inland) along with the use of HYSPLIT and NAAPS reanalysis data. The results
533 reveal notable features that are important for both regulatory purposes and general understanding of aerosol
534 transport and formation processes.
535

536 • The pollution event stemmed from westerly transport under meteorological conditions that promoted
537   secondary inorganic aerosol production in Incheon and Seoul.
538 • Seoul exhibited significantly higher PM$_{2.5}$ levels than Incheon during the polluted period with the
539   difference arising from some combination of local emissions and extensive secondary aerosol formation
540   due to favorable environmental conditions: low temperatures, elevated q and RH, and a shallow boundary
541   layer.
542 • Secondarily produced inorganic and organic acids exhibited significant mass concentrations above 0.94
543   μm during the polluted period (~40% of total mass), and their size-resolved concentrations were highly
544   correlated ($0.94 \leq r \leq 1.00$). The lack of coarse particle influence in promoting concentrations of species
545   like SO$_4^{2-}$, NO$_3^-$, NH$_4^+$, and oxalate provided added support for the role of secondary aerosol formation
546   assisted by high humidity. PM$_{2.5}$ at Seoul and Incheon were best related to q and RH as compared to
547   other examined meteorological parameters. The higher humidities during the polluted period were
548   coincident with increased sulfur and nitrogen oxidation ratios. This highlights the importance of
549   heterogeneous processing and hygroscopic growth in contributing to the high supermicrometer
550   concentrations of inorganic and organic acids in the polluted period. Increased particle size with
551   hygroscopic growth in the humid conditions likely led to increased chemical uptake.
552 • Atypically high values of both NO$_3^-$ mass and NO$_3^-$:SO$_4^{2-}$ mass ratios were observed at both Incheon and
553   Seoul, likely due to low temperatures promoting efficient NO$_3^-$ formation.
554
555   The size distribution information from this work addresses specific concerns that have been raised about
556 the applicability of PM$_1$ composition datasets to understanding PM$_{2.5}$ air quality exceedances in East Asian haze
557 events. Here, we show that PM$_{2.5}$ composition apportionment for water-soluble ions is fully captured by the PM$_1$
558 fraction for haze pollution. Greater differences in the composition apportionment were observed for other
559 atmospheric conditions. The contrast in the dominance of NO$_3^-$ here (March 2019, $T \approx 9°C$) versus the comparable
560 amounts of NO$_3^-$ and SO$_4^{2-}$ observed during the KORUS-AQ campaign haze event (May 2016, $T \approx 20°C$) points
561 to the importance of conducting measurements at different times of the year to more fully understand haze
562 formation and its impacts on air quality. Equally important is the use of these data to rigorously test apportionment
563 of PM$_{2.5}$ composition in air quality models to ensure that the integrated impacts of transport and enhanced
564 chemistry are adequately represented. This work contributes to the growing body of data required for ongoing
565 model assessments of PM$_{2.5}$ that will inform mitigation strategies to improve air quality in South Korea.
566

567 *Data Availability*.
568 The sampled aerosol and meteorological data used in this study can be accessed at
569 https://doi.org/10.6084/m9.figshare.16910686.v1. The NAAPS data used in this study can be accessed at
570 https://nrlgodae1.nrlmry.navy.mil/cgi-bin/datalist.pl?dset=nrl_naaps_reanalysis&summary=Go.
571

572 *Author contributions*.
573 Joseph Schlosser performed the analysis and Joseph Schlosser and Armin Sorooshian prepared the manuscript.
574 Jong-sang Youn, Connor Stahl, and Yen Thi-Hoang Le, Hye-Jung Shin, and In-ho Song conducted sample
575 collection and/or analysis. All authors provided editorial support.

576

577 *Competing interests.*
578 The authors declare that they have no conflict of interest.
579
580 *Acknowledgements.*
581 Incheon (Inha University) data were provided by the Particle Pollution Research and Management Center. Seoul
582 monitoring data were provided by the National Institute of Environmental Research (NIER, NIER-2021-03-03-
583 001). We acknowledge the use of imagery from the NASA Worldview application
584 (https://worldview.earthdata.nasa.gov), part of the NASA Earth Observing System Data and Information System
585 (EOSDIS). The authors acknowledge the NOAA Air Resources Laboratory (ARL) for the provision of the
586 HYSPLIT transport and dispersion model and READY website (http://ready.arl.noaa.gov, last access: 27 October
587 2021) used in this work.

588
589 *Financial Support.*
590 This research was supported by the FRIEND (Fine Particle Research Initiative in East Asia Considering National
591 Differences) Project through the National Research Foundation of Korea (NRF) funded by the Ministry of Science
592 and ICT. (2020M3G1A1114626). Data analysis was funded by ONR grants N00014-21-1-2115 and
593 N0001421WX00227. In addition, this work was supported by the Catholic University of Korea, Research Fund,
594 2021.

595

596 References

597 Aldhaif, A. M., Lopez, D. H., Dadashazar, H., Painemal, D., Peters, A. J., and Sorooshian, A.: An Aerosol
598 Climatology and Implications for Clouds at a Remote Marine Site: Case Study Over Bermuda, J. Geophys. Res.
599 Atmos., 126, e2020JD034038, https://doi.org/10.1029/2020JD034038, 2021.

600 Arimoto, R., Duce, R. A., Savoie, D. L., and Prospero, J. M.: Trace elements in aerosol particles from Bermuda
601 and Barbados: Concentrations, sources and relationships to aerosol sulfate, J. Atmos. Chem., 14, 439-457,
602 10.1007/BF00115250, 1992.

603 AzadiAghdam, M., Braun, R. A., Edwards, E.-L., Bañaga, P. A., Cruz, M. T., Betito, G., Cambaliza, M. O.,
604 Dadashazar, H., Lorenzo, G. R., Ma, L., MacDonald, A. B., Nguyen, P., Simpas, J. B., Stahl, C., and Sorooshian,
605 A.: On the nature of sea salt aerosol at a coastal megacity: Insights from Manila, Philippines in Southeast Asia,
606 Atmos. Environ., 216, 116922, https://doi.org/10.1016/j.atmosenv.2019.116922, 2019.

607 Bolton, D.: The Computation of Equivalent Potential Temperature, Monthly Weather Review, 108, 1046-1053,
608 10.1175/1520-0493(1980)108<1046:tcoept>2.0.co;2, 1980.

609 Cha, Y., Lee, S., and Lee, J.: Measurement of Black Carbon Concentration and Comparison with PM10 and PM2.5
610 Concentrations Monitored in Chungcheong Province, Korea, Aerosol Air Qual. Res., 19, 541-547,
611 10.4209/aaqr.2018.08.0325, 2019.

612 Chen, Y., Wild, O., Wang, Y., Ran, L., Teich, M., Größ, J., Wang, L., Spindler, G., Herrmann, H., van Pinxteren,
613 D., McFiggans, G., and Wiedensohler, A.: The influence of impactor size cut-off shift caused by hygroscopic
614 growth on particulate matter loading and composition measurements, Atmospheric Environment, 195, 141-148,
615 https://doi.org/10.1016/j.atmosenv.2018.09.049, 2018.

616 Cheng, Y., Zheng, G., Wei, C., Mu, Q., Zheng, B., Wang, Z., Gao, M., Zhang, Q., He, K., Carmichael, G., Pöschl,
617 U., and Su, H.: Reactive nitrogen chemistry in aerosol water as a source of sulfate during haze events in China,
618 Sci. Adv., 2, e1601530, 10.1126/sciadv.1601530, 2016.

619 Cho, J. H., Kim, H. S., and Chung, Y. S.: Spatio-temporal changes of PM10 trends in South Korea caused by East
620 Asian atmospheric variability, Air Qual. Atmos. Health, 14, 1001-1016, 10.1007/s11869-021-00995-y, 2021.

621 Choi, J., Park, R. J., Lee, H.-M., Lee, S., Jo, D. S., Jeong, J. I., Henze, D. K., Woo, J.-H., Ban, S.-J., Lee, M.-D.,
622 Lim, C.-S., Park, M.-K., Shin, H. J., Cho, S., Peterson, D., and Song, C.-K.: Impacts of local vs. trans-boundary
623 emissions from different sectors on PM2.5 exposure in South Korea during the KORUS-AQ campaign, Atmos.
624 Environ., 203, 196-205, https://doi.org/10.1016/j.atmosenv.2019.02.008, 2019a.

625 Choi, M., Lim, H., Kim, J., Lee, S., Eck, T. F., Holben, B. N., Garay, M. J., Hyer, E. J., Saide, P. E., and Liu, H.:
626 Validation, comparison, and integration of GOCI, AHI, MODIS, MISR, and VIIRS aerosol optical depth over
627 East Asia during the 2016 KORUS-AQ campaign, Atmos. Meas. Tech., 12, 4619-4641, 10.5194/amt-12-4619-
628 2019, 2019b.

629 Colbeck, I., and Harrison, R. M.: Ozone—secondary aerosol—visibility relationships in North-West England, Sci.
630 Total Environ., 34, 87-100, 1984.

631 Crosbie, E., Sorooshian, A., Monfared, N. A., Shingler, T., and Esmaili, O.: A Multi-Year Aerosol Characterization
632 for the Greater Tehran Area Using Satellite, Surface, and Modeling Data, Atmosphere, 5, 178-197, 2014.

633 Cruz, M. T., Bañaga, P. A., Betito, G., Braun, R. A., Stahl, C., Aghdam, M. A., Cambaliza, M. O., Dadashazar, H.,
634 Hilario, M. R., Lorenzo, G. R., Ma, L., MacDonald, A. B., Pabroa, P. C., Yee, J. R., Simpas, J. B., and Sorooshian,
635 A.: Size-resolved composition and morphology of particulate matter during the southwest monsoon in Metro
636 Manila, Philippines, Atmos. Chem. Phys., 19, 10675-10696, 10.5194/acp-19-10675-2019, 2019.

637 Dadashazar, H., Alipanah, M., Hilario, M. R. A., Crosbie, E., Kirschler, S., Liu, H., Moore, R. H., Peters, A. J.,
638 Scarino, A. J., Shook, M., Thornhill, K. L., Voigt, C., Wang, H., Winstead, E., Zhang, B., Ziemba, L., and
639 Sorooshian, A.: Aerosol Responses to Precipitation Along North American Air Trajectories Arriving at Bermuda,
640 Atmos. Chem. Phys. Discuss., 2021, 1-34, 10.5194/acp-2021-471, 2021.

641 Eck, T. F., Holben, B. N., Kim, J., Beyersdorf, A. J., Choi, M., Lee, S., Koo, J. H., Giles, D. M., Schafer, J. S.,
642 Sinyuk, A., Peterson, D. A., Reid, J. S., Arola, A., Slutsker, I., Smirnov, A., Sorokin, M., Kraft, J., Crawford, J. H.,
643 Anderson, B. E., Thornhill, K. L., Diskin, G., Kim, S.-W., and Park, S.: Influence of cloud, fog, and high relative
644 humidity during pollution transport events in South Korea: Aerosol properties and PM2.5 variability, Atmos.
645 Environ., 232, 117530, https://doi.org/10.1016/j.atmosenv.2020.117530, 2020.

646 Ervens, B., Feingold, G., Frost, G. J., and Kreidenweis, S. M.: A modeling study of aqueous production of
647 dicarboxylic acids: 1. Chemical pathways and speciated organic mass production, J. Geophys. Res. Atmos., 109,
648 https://doi.org/10.1029/2003JD004387, 2004.

649 Fishman, J., and Seiler, W.: Correlative nature of ozone and carbon monoxide in the troposphere: Implications for
650 the tropospheric ozone budget, J. Geophys. Res. Oceans, 88, 3662-3670,
651 https://doi.org/10.1029/JC088iC06p03662, 1983.

652 Gelaro, R., McCarty, W., Suárez, M. J., Todling, R., Molod, A., Takacs, L., Randles, C., Darmenov, A., Bosilovich,
653 M. G., Reichle, R., Wargan, K., Coy, L., Cullather, R., Draper, C., Akella, S., Buchard, V., Conaty, A., da Silva,
654 A., Gu, W., Kim, G.-K., Koster, R., Lucchesi, R., Merkova, D., Nielsen, J. E., Partyka, G., Pawson, S., Putman,
655 W., Rienecker, M., Schubert, S. D., Sienkiewicz, M., and Zhao, B.: The Modern-Era Retrospective Analysis for
656 Research and Applications, Version 2 (MERRA-2), J. Clim., Volume 30, 5419-5454, 10.1175/JCLI-D-16-0758.1,
657 2017.
658 GMAO: MERRA-2 tavg1_2d_flx_Nx: 2d,1-Hourly,Time-Averaged,Single-Level,Assimilation,Surface Flux
659 Diagnostics V5.12.4, in, edited by: DISC), G. E. S. D. a. I. S. C. G., Greenbelt, MD, 2015.
660 Guttikunda, S. K., Carmichael, G. R., Calori, G., Eck, C., and Woo, J.-H.: The contribution of megacities to
661 regional sulfur pollution in Asia, Atmos. Environ., 37, 11-22, https://doi.org/10.1016/S1352-2310(02)00821-X,
662 2003.
663 Halliday, H. S., DiGangi, J. P., Choi, Y., Diskin, G. S., Pusede, S. E., Rana, M., Nowak, J. B., Knote, C., Ren, X.,
664 He, H., Dickerson, R. R., and Li, Z.: Using Short-Term CO/CO2 Ratios to Assess Air Mass Differences Over the
665 Korean Peninsula During KORUS-AQ, J. Geophys. Res. Atmos., 124, 10951-10972,
666 https://doi.org/10.1029/2018JD029697, 2019.
667 Heim, E. W., Dibb, J., Scheuer, E., Jost, P. C., Nault, B. A., Jimenez, J. L., Peterson, D., Knote, C., Fenn, M., Hair,
668 J., Beyersdorf, A. J., Corr, C., and Anderson, B. E.: Asian dust observed during KORUS-AQ facilitates the uptake
669 and incorporation of soluble pollutants during transport to South Korea, Atmos. Environ., 224, 117305,
670 https://doi.org/10.1016/j.atmosenv.2020.117305, 2020.
671 Hennigan, C. J., Bergin, M. H., Dibb, J. E., and Weber, R. J.: Enhanced secondary organic aerosol formation due
672 to water uptake by fine particles, Geophys. Res. Lett., 35, https://doi.org/10.1029/2008GL035046, 2008.
673 Hennigan, C. J., Bergin, M. H., Russell, A. G., Nenes, A., and Weber, R. J.: Gas/particle partitioning of water-
674 soluble organic aerosol in Atlanta, Atmos. Chem. Phys., 9, 3613-3628, 10.5194/acp-9-3613-2009, 2009.
675 Hersey, S. P., Garland, R. M., Crosbie, E., Shingler, T., Sorooshian, A., Piketh, S., and Burger, R.: An overview of
676 regional and local characteristics of aerosols in South Africa using satellite, ground, and modeling data, Atmos.
677 Chem. Phys., 15, 4259-4278, 10.5194/acp-15-4259-2015, 2015.
678 Hilario, M. R. A., Crosbie, E., Bañaga, P. A., Betito, G., Braun, R. A., Cambaliza, M. O., Corral, A. F., Cruz, M.
679 T., Dibb, J. E., Lorenzo, G. R., MacDonald, A. B., Robinson, C. E., Shook, M. A., Simpas, J. B., Stahl, C.,
680 Winstead, E., Ziemba, L. D., and Sorooshian, A.: Particulate Oxalate-To-Sulfate Ratio as an Aqueous Processing
681 Marker: Similarity Across Field Campaigns and Limitations, Geophys. Res. Lett., 48, e2021GL096520,
682 https://doi.org/10.1029/2021GL096520, 2021a.
683 Hilario, M. R. A., Crosbie, E., Shook, M., Reid, J. S., Cambaliza, M. O. L., Simpas, J. B. B., Ziemba, L., DiGangi,
684 J. P., Diskin, G. S., Nguyen, P., Turk, F. J., Winstead, E., Robinson, C. E., Wang, J., Zhang, J., Wang, Y., Yoon, S.,
685 Flynn, J., Alvarez, S. L., Behrangi, A., and Sorooshian, A.: Measurement report: Long-range transport patterns
686 into the tropical northwest Pacific during the CAMP2Ex aircraft campaign: chemical composition, size
687 distributions, and the impact of convection, Atmos. Chem. Phys., 21, 3777-3802, 10.5194/acp-21-3777-2021,
688 2021b.
689 Hogan, T. F., Liu, M., Ridout, J. A., Peng, M. S., Whitcomb, T. R., Ruston, B. C., Reynolds, C. A., Eckermann, S.
690 D., Moskaitis, J. R., Baker, N. L., McCormack, J. P., Viner, K. C., McLay, J. G., Flatau, M. K., Xu, L., Chen, C.,
691 and Chang, S. W.: The Navy Global Environmental Model, Oceanography, 27, 116-125, 2014.
692 Hu, J., Wang, Y., Ying, Q., and Zhang, H.: Spatial and temporal variability of PM2.5 and PM10 over the North
693 China Plain and the Yangtze River Delta, China, Atmos. Environ., 95, 598-609,
694 https://doi.org/10.1016/j.atmosenv.2014.07.019, 2014.
695 Huang, R.-J., Zhang, Y., Bozzetti, C., Ho, K.-F., Cao, J.-J., Han, Y., Daellenbach, K. R., Slowik, J. G., Platt, S. M.,
696 Canonaco, F., Zotter, P., Wolf, R., Pieber, S. M., Bruns, E. A., Crippa, M., Ciarelli, G., Piazzalunga, A.,
697 Schwikowski, M., Abbaszade, G., Schnelle-Kreis, J., Zimmermann, R., An, Z., Szidat, S., Baltensperger, U.,
698 Haddad, I. E., and Prévôt, A. S. H.: High secondary aerosol contribution to particulate pollution during haze events
699 in China, Nature, 514, 218-222, 10.1038/nature13774, 2014.
700 Huang, R. J., He, Y., Duan, J., Li, Y., Chen, Q., Zheng, Y., Chen, Y., Hu, W., Lin, C., Ni, H., Dai, W., Cao, J., Wu,
701 Y., Zhang, R., Xu, W., Ovadnevaite, J., Ceburnis, D., Hoffmann, T., and O'Dowd, C. D.: Contrasting sources and
702 processes of particulate species in haze days with low and high relative humidity in wintertime Beijing, Atmos.
703 Chem. Phys., 20, 9101-9114, 10.5194/acp-20-9101-2020, 2020.
704 Hyer, E. J., Reid, J. S., and Zhang, J.: An over-land aerosol optical depth data set for data assimilation by filtering,
705 correction, and aggregation of MODIS Collection 5 optical depth retrievals, Atmos. Meas. Tech., 4, 379-408,
706 10.5194/amt-4-379-2011, 2011.
707 Jeon, W., Park, J., Choi, Y., Mun, J., Kim, D., Kim, C.-H., Lee, H.-J., Bak, J., and Jo, H.-Y.: The mechanism of
708 the formation of high sulfate concentrations over the Yellow Sea during the KORUS-AQ period: The effect of

709 transport/atmospheric chemistry and ocean emissions, Atmos. Res., 105756,
710 https://doi.org/10.1016/j.atmosres.2021.105756, 2021.
711 Ji, Y., Qin, X., Wang, B., Xu, J., Shen, J., Chen, J., Huang, K., Deng, C., Yan, R., Xu, K., and Zhang, T.:
712 Counteractive effects of regional transport and emission control on the formation of fine particles: a case study
713 during the Hangzhou G20 summit, Atmos. Chem. Phys., 18, 13581-13600, 10.5194/acp-18-13581-2018, 2018.
714 Jordan, C. E., Crawford, J. H., Beyersdorf, A. J., Eck, T. F., Halliday, H. S., Nault, B. A., Chang, L.-S., Park, J.,
715 Park, R., Lee, G., Kim, H., Ahn, J.-y., Cho, S., Shin, H. J., Lee, J. H., Jung, J., Kim, D.-S., Lee, M., Lee, T.,
716 Whitehill, A., Szykman, J., Schueneman, M. K., Campuzano-Jost, P., Jimenez, J. L., DiGangi, J. P., Diskin, G. S.,
717 Anderson, B. E., Moore, R. H., Ziemba, L. D., Fenn, M. A., Hair, J. W., Kuehn, R. E., Holz, R. E., Chen, G.,
718 Travis, K., Shook, M., Peterson, D. A., Lamb, K. D., and Schwarz, J. P.: Investigation of factors controlling PM2.5
719 variability across the South Korean Peninsula during KORUS-AQ, Elementa, 8, 10.1525/elementa.424, 2020.
720 Kaneyasu, N., Ohta, S., and Murao, N.: Seasonal variation in the chemical composition of atmospheric aerosols
721 and gaseous species in Sapporo, Japan, Atmos. Environ., 29, 1559-1568, https://doi.org/10.1016/1352-
722 2310(94)00356-P, 1995.
723 Kim, H.-S., Chung, Y.-S., and Lee, S.-G.: Characteristics of aerosol types during large-scale transport of air
724 pollution over the Yellow Sea region and at Cheongwon, Korea, in 2008, Environ. Monit. Assess., 184, 1973-
725 1984, 10.1007/s10661-011-2092-9, 2012.
726 Kim, Y. P., and Lee, G.: Trend of Air Quality in Seoul: Policy and Science, Aerosol Air Qual. Res., 18, 2141-2156,
727 10.4209/aaqr.2018.03.0081, 2018.
728 Koo, J.-H., Kim, J., Lee, Y. G., Park, S. S., Lee, S., Chong, H., Cho, Y., Kim, J., Choi, K., and Lee, T.: The
729 implication of the air quality pattern in South Korea after the COVID-19 outbreak, Sci. Rep., 10, 22462,
730 10.1038/s41598-020-80429-4, 2020.
731 Koo, Y.-S., Yun, H.-Y., Choi, D.-R., Han, J.-S., Lee, J.-B., and Lim, Y.-J.: An analysis of chemical and
732 meteorological characteristics of haze events in the Seoul metropolitan area during January 12–18, 2013, Atmos.
733 Environ., 178, 87-100, https://doi.org/10.1016/j.atmosenv.2018.01.037, 2018.
734 Population Statistics: https://kosis.kr/statHtml/statHtml.do?orgId=101&tblId=DT_1B040A3, 2021.
735 Lamb, K. D., Perring, A. E., Samset, B., Peterson, D., Davis, S., Anderson, B. E., Beyersdorf, A., Blake, D. R.,
736 Campuzano-Jost, P., Corr, C. A., Diskin, G. S., Kondo, Y., Moteki, N., Nault, B. A., Oh, J., Park, M., Pusede, S.
737 E., Simpson, I. J., Thornhill, K. L., Wisthaler, A., and Schwarz, J. P.: Estimating Source Region Influences on
738 Black Carbon Abundance, Microphysics, and Radiative Effect Observed Over South Korea, J. Geophys. Res.
739 Atmos., 123, 13,527-513,548, https://doi.org/10.1029/2018JD029257, 2018.
740 Lee, D., Choi, J.-Y., Myoung, J., Kim, O., Park, J., Shin, H.-J., Ban, S.-J., Park, H.-J., and Nam, K.-P.: Analysis
741 of a Severe PM2.5 Episode in the Seoul Metropolitan Area in South Korea from 27 February to 7 March 2019:
742 Focused on Estimation of Domestic and Foreign Contribution, Atmosphere, 10, 756, 2019a.
743 Lee, J. Y., and Kim, Y. P.: Source apportionment of the particulate PAHs at Seoul, Korea: impact of long range
744 transport to a megacity, Atmos. Chem. Phys., 7, 3587-3596, 10.5194/acp-7-3587-2007, 2007.
745 Lee, S., Hong, J., Cho, Y., Choi, M., Kim, J., Park, S. S., Ahn, J.-Y., Kim, S.-K., Moon, K.-J., Eck, T. F., Holben,
746 B. N., and Koo, J.-H.: Characteristics of Classified Aerosol Types in South Korea during the MAPS-Seoul
747 Campaign, Aerosol Air Qual. Res., 18, 2195-2206, 10.4209/aaqr.2017.11.0474, 2018.
748 Lee, S., Kim, J., Choi, M., Hong, J., Lim, H., Eck, T. F., Holben, B. N., Ahn, J.-Y., Kim, J., and Koo, J.-H.:
749 Analysis of long-range transboundary transport (LRTT) effect on Korean aerosol pollution during the KORUS-
750 AQ campaign, Atmos. Environ., 204, 53-67, https://doi.org/10.1016/j.atmosenv.2019.02.020, 2019b.
751 Lee, S., Kim, M., Kim, S.-Y., Lee, D.-W., Lee, H., Kim, J., Le, S., and Liu, Y.: Assessment of long-range
752 transboundary aerosols in Seoul, South Korea from Geostationary Ocean Color Imager (GOCI) and ground-based
753 observations, Environ. Pollut., 269, 115924, https://doi.org/10.1016/j.envpol.2020.115924, 2021.
754 Lee, Y.-N., Weber, R., Ma, Y., Orsini, D., Maxwell-Meier, K., Blake, D., Meinardi, S., Sachse, G., Harward, C.,
755 Chen, T.-Y., Thornton, D., Tu, F.-H., and Bandy, A.: Airborne measurement of inorganic ionic components of fine
756 aerosol particles using the particle-into-liquid sampler coupled to ion chromatography technique during ACE-
757 Asia and TRACE-P, J. Geophys. Res. Atmos., 108, https://doi.org/10.1029/2002JD003265, 2003.
758 Lennartson, E. M., Wang, J., Gu, J., Castro Garcia, L., Ge, C., Gao, M., Choi, M., Saide, P. E., Carmichael, G. R.,
759 Kim, J., and Janz, S. J.: Diurnal variation of aerosol optical depth and PM2.5 in South Korea: a synthesis from
760 AERONET, satellite (GOCI), KORUS-AQ observation, and the WRF-Chem model, Atmos. Chem. Phys., 18,
761 15125-15144, 10.5194/acp-18-15125-2018, 2018.
762 Li, J., Zhang, Y.-L., Cao, F., Zhang, W., Fan, M., Lee, X., and Michalski, G.: Stable Sulfur Isotopes Revealed a
763 Major Role of Transition-Metal Ion-Catalyzed SO2 Oxidation in Haze Episodes, Environ. Sci. Technol., 54, 2626-
764 2634, 10.1021/acs.est.9b07150, 2020.

765 Li, K., Chen, L., White, S. J., Zheng, X., Lv, B., Lin, C., Bao, Z., Wu, X., Gao, X., Ying, F., Shen, J., Azzi, M.,
766 and Cen, K.: Chemical characteristics and sources of PM1 during the 2016 summer in Hangzhou, Environ. Pollut.,
767 232, 42-54, https://doi.org/10.1016/j.envpol.2017.09.016, 2018.
768 Lynch, P., Reid, J. S., Westphal, D. L., Zhang, J., Hogan, T. F., Hyer, E. J., Curtis, C. A., Hegg, D. A., Shi, Y.,
769 Campbell, J. R., Rubin, J. I., Sessions, W. R., Turk, F. J., and Walker, A. L.: An 11-year global gridded aerosol
770 optical thickness reanalysis (v1.0) for atmospheric and climate sciences, Geosci. Model Dev., 9, 1489-1522,
771 10.5194/gmd-9-1489-2016, 2016.
772 MacDonald, A. B., Dadashazar, H., Chuang, P. Y., Crosbie, E., Wang, H., Wang, Z., Jonsson, H. H., Flagan, R. C.,
773 Seinfeld, J. H., and Sorooshian, A.: Characteristic Vertical Profiles of Cloud Water Composition in Marine
774 Stratocumulus Clouds and Relationships With Precipitation, J. Geophys. Res. Atmos., 123, 3704-3723,
775 https://doi.org/10.1002/2017JD027900, 2018.
776 Maudlin, L. C., Wang, Z., Jonsson, H. H., and Sorooshian, A.: Impact of wildfires on size-resolved aerosol
777 composition at a coastal California site, Atmos. Environ., 119, 59-68,
778 https://doi.org/10.1016/j.atmosenv.2015.08.039, 2015.
779 Mora, M., Braun, R. A., Shingler, T., and Sorooshian, A.: Analysis of remotely sensed and surface data of aerosols
780 and meteorology for the Mexico Megalopolis Area between 2003 and 2015, J. Geophys. Res. Atmos., 122, 8705-
781 8723, https://doi.org/10.1002/2017JD026739, 2017.
782 Nault, B. A., Campuzano-Jost, P., Day, D. A., Schroder, J. C., Anderson, B., Beyersdorf, A. J., Blake, D. R., Brune,
783 W. H., Choi, Y., Corr, C. A., de Gouw, J. A., Dibb, J., DiGangi, J. P., Diskin, G. S., Fried, A., Huey, L. G., Kim,
784 M. J., Knote, C. J., Lamb, K. D., Lee, T., Park, T., Pusede, S. E., Scheuer, E., Thornhill, K. L., Woo, J. H., and
785 Jimenez, J. L.: Secondary organic aerosol production from local emissions dominates the organic aerosol budget
786 over Seoul, South Korea, during KORUS-AQ, Atmos. Chem. Phys., 18, 17769-17800, 10.5194/acp-18-17769-
787 2018, 2018.
788 Paciga, A. L., Riipinen, I., and Pandis, S. N.: Effect of Ammonia on the Volatility of Organic Diacids, Environ.
789 Sci. Technol., 48, 13769-13775, 10.1021/es5037805, 2014.
790 Park, G., Kim, K., Park, T., Kang, S., Ban, J., Choi, S., Yu, D.-G., Lee, S., Lim, Y., Kim, S., Mun, S., Woo, J.-H.,
791 Jeon, C.-S., and Lee, T.: Primary and secondary aerosols in small passenger vehicle emissions: Evaluation of
792 engine technology, driving conditions, and regulatory standards, Environ. Pollut., 286, 117195,
793 https://doi.org/10.1016/j.envpol.2021.117195, 2021.
794 Park, I.-S., Park, M.-S., Jang, Y. W., Kim, H.-K., Song, C.-K., Owen, J. S., Kim, S.-H., Cho, C.-R., and Kim, C.-
795 H.: Impact Comparison of Synoptic Meteorology and Nationwide/local Emissions on the Seoul Metropolitan Area
796 during High PM Multi-event and Non-event Days, 10.5572/ajae.2020.14.3.263, 2020a.
797 Park, S.-M., Song, I.-H., Park, J. S., Oh, J., Moon, K. J., Shin, H. J., Ahn, J. Y., Lee, M.-D., Kim, J., and Lee, G.:
798 Variation of PM2.5 Chemical Compositions and their Contributions to Light Extinction in Seoul, Aerosol Air Qual.
799 Res., 18, 2220-2229, 10.4209/aaqr.2017.10.0369, 2018.
800 Park, S., Thi Hong, H. D., Cho, S. Y., and Bae, M.-S.: Chemical Composition and Light Absorption of PM2.5
801 Observed at Two Sites near a Busy Road during Summer and Winter, Appl. Sci., 10, 4858, 2020b.
802 Peterson, D. A., Hyer, E. J., Han, S.-O., Crawford, J. H., Park, R. J., Holz, R., Kuehn, R. E., Eloranta, E., Knote,
803 C., Jordan, C. E., and Lefer, B. L.: Meteorology influencing springtime air quality, pollution transport, and
804 visibility in Korea, Elementa, 7, 10.1525/elementa.395, 2019.
805 Quan, J., Liu, Q., Li, X., Gao, Y., Jia, X., Sheng, J., and Liu, Y.: Effect of heterogeneous aqueous reactions on the
806 secondary formation of inorganic aerosols during haze events, Atmos. Environ., 122, 306-312,
807 https://doi.org/10.1016/j.atmosenv.2015.09.068, 2015.
808 Rolph, G., Stein, A., and Stunder, B.: Real-time Environmental Applications and Display sYstem: READY,
809 Environ. Model Softw., 95, 210-228, https://doi.org/10.1016/j.envsoft.2017.06.025, 2017.
810 Ryu, Y.-H., and Min, S.-K.: Long-term evaluation of atmospheric composition reanalyses from CAMS, TCR-2,
811 and MERRA-2 over South Korea: Insights into applications, implications, and limitations, Atmos. Environ., 246,
812 118062, https://doi.org/10.1016/j.atmosenv.2020.118062, 2021.
813 Ryu, Y.-H., Min, S.-K., and Hodzic, A.: Recent Decreasing Trends in Surface PM2.5 over East Asia in the Winter-
814 spring Season: Different Responses to Emissions and Meteorology between Upwind and Downwind Regions,
815 Aerosol Air Qual. Res., 21, 200654, 10.4209/aaqr.200654, 2021.
816 Seinfeld, J. H., and Pandis, S. N.: Atmospheric Chemistry and Physics, 3 ed., Wiley-Interscience, New York, 2016.
817 Seo, J., Park, D. S. R., Kim, J. Y., Youn, D., Lim, Y. B., and Kim, Y.: Effects of meteorology and emissions on
818 urban air quality: a quantitative statistical approach to long-term records (1999–2016) in Seoul, South Korea,
819 Atmos. Chem. Phys., 18, 16121-16137, 10.5194/acp-18-16121-2018, 2018.

820 Seo, J., Lim, Y. B., Youn, D., Kim, J. Y., and Jin, H. C.: Synergistic enhancement of urban haze by nitrate uptake
821 into transported hygroscopic particles in the Asian continental outflow, Atmos. Chem. Phys., 20, 7575-7594,
822 10.5194/acp-20-7575-2020, 2020.
823 Shao, J., Chen, Q., Wang, Y., Lu, X., He, P., Sun, Y., Shah, V., Martin, R. V., Philip, S., Song, S., Zhao, Y., Xie, Z.,
824 Zhang, L., and Alexander, B.: Heterogeneous sulfate aerosol formation mechanisms during wintertime Chinese
825 haze events: air quality model assessment using observations of sulfate oxygen isotopes in Beijing, Atmos. Chem.
826 Phys., 19, 6107-6123, 10.5194/acp-19-6107-2019, 2019.
827 Sorooshian, A., Varutbangkul, V., Brechtel, F. J., Ervens, B., Feingold, G., Bahreini, R., Murphy, S. M., Holloway,
828 J. S., Atlas, E. L., Buzorius, G., Jonsson, H., Flagan, R. C., and Seinfeld, J. H.: Oxalic acid in clear and cloudy
829 atmospheres: Analysis of data from International Consortium for Atmospheric Research on Transport and
830 Transformation 2004, J. Geophys. Res. Atmos., 111, https://doi.org/10.1029/2005JD006880, 2006.
831 Sorooshian, A., Lu, M.-L., Brechtel, F. J., Jonsson, H., Feingold, G., Flagan, R. C., and Seinfeld, J. H.: On the
832 Source of Organic Acid Aerosol Layers above Clouds, Environ. Sci. Technol., 41, 4647-4654, 10.1021/es0630442,
833 2007.
834 Sorooshian, A., Murphy, S. M., Hersey, S., Bahreini, R., Jonsson, H., Flagan, R. C., and Seinfeld, J. H.:
835 Constraining the contribution of organic acids and AMS m/z 44 to the organic aerosol budget: On the importance
836 of meteorology, aerosol hygroscopicity, and region, Geophys. Res. Lett., 37,
837 https://doi.org/10.1029/2010GL044951, 2010.
838 Stahl, C., Cruz, M. T., Bañaga, P. A., Betito, G., Braun, R. A., Aghdam, M. A., Cambaliza, M. O., Lorenzo, G. R.,
839 MacDonald, A. B., Pabroa, P. C., Yee, J. R., Simpas, J. B., and Sorooshian, A.: An annual time series of weekly
840 size-resolved aerosol properties in the megacity of Metro Manila, Philippines, Sci. Data, 7, 128, 10.1038/s41597-
841 020-0466-y, 2020.
842 Stein, A. F., Draxler, R. R., Rolph, G. D., Stunder, B. J. B., Cohen, M. D., and Ngan, F.: NOAA's hysplit
843 atmospheric transport and dispersion modeling system, in: Bull. Am. Meteorol. Soc., 12, 2059+, 2015.
844 Wang, G., Zhang, R., Gomez, M. E., Yang, L., Levy Zamora, M., Hu, M., Lin, Y., Peng, J., Guo, S., Meng, J., Li,
845 J., Cheng, C., Hu, T., Ren, Y., Wang, Y., Gao, J., Cao, J., An, Z., Zhou, W., Li, G., Wang, J., Tian, P., Marrero-
846 Ortiz, W., Secrest, J., Du, Z., Zheng, J., Shang, D., Zeng, L., Shao, M., Wang, W., Huang, Y., Wang, Y., Zhu, Y.,
847 Li, Y., Hu, J., Pan, B., Cai, L., Cheng, Y., Ji, Y., Zhang, F., Rosenfeld, D., Liss, P. S., Duce, R. A., Kolb, C. E., and
848 Molina, M. J.: Persistent sulfate formation from London Fog to Chinese haze, Proc. Natl. Acad. Sci. U.S.A., 113,
849 13630-13635, 10.1073/pnas.1616540113, 2016.
850 Wang, J., Li, J., Ye, J., Zhao, J., Wu, Y., Hu, J., Liu, D., Nie, D., Shen, F., Huang, X., Huang, D. D., Ji, D., Sun,
851 X., Xu, W., Guo, J., Song, S., Qin, Y., Liu, P., Turner, J. R., Lee, H. C., Hwang, S., Liao, H., Martin, S. T., Zhang,
852 Q., Chen, M., Sun, Y., Ge, X., and Jacob, D. J.: Fast sulfate formation from oxidation of SO2 by NO2 and HONO
853 observed in Beijing haze, Nat. Commun., 11, 2844, 10.1038/s41467-020-16683-x, 2020.
854 Weinstock, B.: Carbon Monoxide: Residence Time in the Atmosphere, Science, 166, 224-225,
855 doi:10.1126/science.166.3902.224, 1969.
856 Won, W.-S., Oh, R., Lee, W., Kim, K.-Y., Ku, S., Su, P.-C., and Yoon, Y.-J.: Impact of Fine Particulate Matter on
857 Visibility at Incheon International Airport, South Korea, Aerosol Air Qual. Res., 1048-1061,
858 10.4209/aaqr.2019.03.0106, 2020.
859 Wonaschuetz, A., Sorooshian, A., Ervens, B., Chuang, P. Y., Feingold, G., Murphy, S. M., de Gouw, J., Warneke,
860 C., and Jonsson, H. H.: Aerosol and gas re-distribution by shallow cumulus clouds: An investigation using airborne
861 measurements, J. Geophys. Res. Atmos., 117, https://doi.org/10.1029/2012JD018089, 2012.
862 Wu, Y., Ge, X., Wang, J., Shen, Y., Ye, Z., Ge, S., Wu, Y., Yu, H., and Chen, M.: Responses of secondary aerosols
863 to relative humidity and photochemical activities in an industrialized environment during late winter, Atmos.
864 Environ., 193, 66-78, https://doi.org/10.1016/j.atmosenv.2018.09.008, 2018.
865 Yang, T., Sun, Y., Zhang, W., Wang, Z., Liu, X., Fu, P., and Wang, X.: Evolutionary processes and sources of high-
866 nitrate haze episodes over Beijing, Spring, J. Environ. Sci., 54, 142-151, https://doi.org/10.1016/j.jes.2016.04.024,
867 2017.
868 Yu, J. Z., Huang, X.-F., Xu, J., and Hu, M.: When Aerosol Sulfate Goes Up, So Does Oxalate: Implication for the
869 Formation Mechanisms of Oxalate, Environ. Sci. Technol., 39, 128-133, 10.1021/es049559f, 2005.
870 Zhang, C., Lu, X., Zhai, J., Chen, H., Yang, X., Zhang, Q., Zhao, Q., Fu, Q., Sha, F., and Jin, J.: Insights into the
871 formation of secondary organic carbon in the summertime in urban Shanghai, J. Environ. Sci., 72, 118-132,
872 https://doi.org/10.1016/j.jes.2017.12.018, 2018.
873 Zhang, J., and Reid, J. S.: MODIS aerosol product analysis for data assimilation: Assessment of over-ocean level
874 2 aerosol optical thickness retrievals, J. Geophys. Res. Atmos., 111, https://doi.org/10.1029/2005JD006898, 2006.

875   Zhang, Q., Worsnop, D. R., Canagaratna, M. R., and Jimenez, J. L.: Hydrocarbon-like and oxygenated organic
876   aerosols in Pittsburgh: insights into sources and processes of organic aerosols, Atmos. Chem. Phys., 5, 3289-3311,
877   10.5194/acp-5-3289-2005, 2005.
878   Zhang, R., Wang, G., Guo, S., Zamora, M. L., Ying, Q., Lin, Y., Wang, W., Hu, M., and Wang, Y.: Formation of
879   Urban Fine Particulate Matter, Chemical Reviews, 115, 3803-3855, 10.1021/acs.chemrev.5b00067, 2015.
880   Zhang, T., Shen, Z. X., Su, H., Liu, S. X., Zhou, J. M., Zhao, Z. Z., Wang, Q. Y., Prévôt, A. S. H., and Cao, J. J.:
881   Effects of Aerosol Water Content on the formation of secondary inorganic aerosol during a Winter Heavy PM2.5
882   Pollution Episode in Xi'an, China, Atmos. Environ., 252, 118304, https://doi.org/10.1016/j.atmosenv.2021.118304,
883   2021.
884   Zhang, Y., Tang, L., Croteau, P. L., Favez, O., Sun, Y., Canagaratna, M. R., Wang, Z., Couvidat, F., Albinet, A.,
885   Zhang, H., Sciare, J., Prévôt, A. S. H., Jayne, J. T., and Worsnop, D. R.: Field characterization of the PM2.5
886   Aerosol Chemical Speciation Monitor: insights into the composition, sources, and processes of fine particles in
887   eastern China, Atmos. Chem. Phys., 17, 14501-14517, 10.5194/acp-17-14501-2017, 2017.
888   Zhou, Y., Huang, X. H., Bian, Q., Griffith, S. M., Louie, P. K. K., and Yu, J. Z.: Sources and atmospheric processes
889   impacting oxalate at a suburban coastal site in Hong Kong: Insights inferred from 1 year hourly measurements, J.
890   Geophys. Res. Atmos., 120, 9772-9788, https://doi.org/10.1002/2015JD023531, 2015.

891